THE UNIVERSITY of EDINBURGH

Edinburgh Research Explorer

Prediction of soil water retention properties using pore-size distribution and porosity

Citation for published version:
Beckett, CTS & Augarde, CE 2013, 'Prediction of soil water retention properties using pore-size distribution and porosity', *Canadian geotechnical journal*, vol. 50, no. 4, pp. 435-450. https://doi.org/10.1139/cgj-2012-0320

Digital Object Identifier (DOI):
10.1139/cgj-2012-0320

Link:
Link to publication record in Edinburgh Research Explorer

Document Version:
Peer reviewed version

Published In:
Canadian geotechnical journal

General rights
Copyright for the publications made accessible via the Edinburgh Research Explorer is retained by the author(s) and / or other copyright owners and it is a condition of accessing these publications that users recognise and abide by the legal requirements associated with these rights.

Take down policy
The University of Edinburgh has made every reasonable effort to ensure that Edinburgh Research Explorer content complies with UK legislation. If you believe that the public display of this file breaches copyright please contact openaccess@ed.ac.uk providing details, and we will remove access to the work immediately and investigate your claim.

Download date: 05. May. 2023

Canadian Geotechnical Journal
Revue canadienne de géotechnique

Prediction of soil water retention properties using pore size distribution and porosity

Journal:	*Canadian Geotechnical Journal*
Manuscript ID:	cgj-2012-0320 .R1
Manuscript Type:	Article
Date Submitted by the Author:	09-Nov-2012
Complete List of Authors:	Beckett, Christopher; University of Western Australia, School of Civil and Resource Engineering Augarde, Charles; Durham University, School of Engineering and Computing Science
Keyword:	Pore size distribution, Suction, Cavitation

SCHOLARONE™
Manuscripts

Prediction of soil water retention properties using pore size distribution and porosity

Christopher T. S. Beckett and Charles E. Augarde

Abstract:

Several models have been suggested to link a soil's pore size distribution to its retention properties. This paper presents a method which builds on previous techniques by incorporating porosity and particles of different sizes, shapes and separation distances to predict soil water retention properties. Mechanisms are suggested for the determination of both the main drying and wetting paths which incorporate an adsorbed water phase and retention hysteresis. Predicted results are then compared to measured retention data in order to validate the model and to provide a foundation for discussing the validity and limitations of using pore size distributions to predict retention properties.

Key words: Pore size distribution; suction; cavitation.

1. Introduction

The soil water retention curve is the relationship between suction and the water content (or degree of saturation) of an unsaturated soil and is a key factor in determining its behaviour (Nuth and Laloui, 2008; Tarantino, 2010; Gens, 2010). Suction arises due to the formation of curved water menisci at the air-water interfaces within soil pores. The simplest example of this effect is the phenomenon of

Received April 10, 2012. Revision received . Accepted . Revision accepted .

C. T. S. Beckett.
School of Civil & Resource Engineering, University of Western Australia, Perth, WA 6009, Australia
C. E. Augarde.
School of Engineering and Computing Sciences, Durham University, Durham, DH1 3LE, UK

 © xxxx NRC Canada

Draft

capillary rise, where water in a free reservoir will spontaneously rise to a height in a thin tube of radius r_{tube}. The corresponding suction, ψ, for a given height rise h is calculated using

$$\psi = u_a - u_w = -h\rho g = -\frac{2\gamma}{\kappa} = -\frac{2\gamma\cos(\theta_{slv})}{r_{tube}} \quad (1)$$

where u_a and u_w are the air and water pressures respectively, γ is the air-water surface tension, θ_{slv} is the solid-liquid contact angle in the presence of a vapour (in this case air) and κ is the meniscus radius of curvature. It is commonly assumed that $\theta_{slv} = 0$, so that the meniscus curvature equals the tube radius, and that $u_a = 0$. This phenomenon, although simplistic, nonetheless demonstrates the direct link between suction and the size of the body (i.e. the pore) in which the water is held.

As the direct determination of a soil's retention properties can be time consuming or difficult, several models have been suggested to relate a soil's pore size distribution (PSD) to its retention properties (Ghanbarian-Alavijeh and Liaghat, 2009). The simplest of these is the Bundle of Cylindrical Capillaries (BCC) model, where each pore size is considered to be a capillary tube of a certain diameter, with suction calculated according to Eqn 1 (Millington and Quirk, 1961; Mualem, 1976). The disadvantage of the basic BCC model, however, is that pores are required to be either completely filled or completely empty, so that the unsaturated soil effectively becomes a combination of a completely dry and a completely saturated material (Tuller and Or, 2004; Baker and Frydman, 2009). Observations of water regimes in unsaturated soils made by Lourenço et al. (2012) using environmental scanning electron microscopy (ESEM) show that water and air exist simultaneously in a pore of a given size, with water occupying both a bulk and an adsorbed phase. Adsorption is the mechanism whereby water molecules readily adhere to the surfaces of soil particles due to short-range solid-water interaction mechanisms (including van der Waals attractions, exchangeable cation hydration and electrical field polarisation) (Philip, 1977; Derjaguin et al., 1987; Lu and Likos, 2004). The presence of adsorbed films in cylindrical pores was considered by Shull (1948) for correcting obtained PSD data from nitrogen adsorption techniques (for example the BET method) and by Collet et al. (2008) for predicting PSDs of hemp-based materials from retention properties determined using vapour-equilibrium, however these works did not then go on to use measured PSDs to predict retention properties.

A more advanced model for predicting retention properties which incorporates both bulk and adsorbed water regimes was suggested by Tuller et al. (1999), wherein pore spaces were assumed to be

©xxxx NRC Canada

Draft

angular voids joined by narrow slits, as shown in Figure 1. The bulk and adsorbed phases were separated for ease of calculation into menisci present in the pore corners and adsorbed films in the narrow slits. The disadvantage of this model, however, is that calculations are dependent on the "angularity factor" of the pores, which is information not usually available (Baker and Frydman, 2009).

An improvement to the model suggested by Tuller et al. (1999) is to consider the geometry and arrangement of soil particles surrounding the pore space as well as the water regime. An example of a water meniscus suspended between two granular soil particles is shown in Figure 2, along with adsorbed films of exaggerated thickness. A meniscus suspended between two particles has both concave and convex curvatures in the meridional and azimuthal directions respectively, properties which are not possible in the model of Tuller et al. (1999) due to the columnar pore assumption (Butt, 2008). Although the shapes of granular particles are complicated, simplifying them allows suctions generated in the suspended menisci to be calculated. Lu and Likos (2004), Mayer and Stowe (2006), Grof et al. (2008) and Likos (2009) suggested models wherein granular particles are assumed to be spherical and in contact, with toroidal menisci suspended between particles of equal size. These assumptions allow suction to be calculated via

$$\psi = \gamma \left(\frac{1}{\kappa} - \frac{1}{l} \right) \tag{2}$$

where κ and l are the meridional and azimuthal radii respectively and are each functions of particle size (these functions will be discussed in a later section) and pore size is assumed to be the diameter of the interstitial sphere, as shown in Figure 3. Water is assumed to exist either in bulk or as menisci suspended between particles and, in the case of Likos (2009), in the form of thin films adsorbed onto the particle surfaces. This paper aims to improve on these models by assuming a more realistic arrangement of soil particles which accounts for material porosity, whilst retaining the effect of adsorbed water on the SWRC introduced in Tuller et al. (1999) and Likos (2009). Predictions made using the model are then compared to measured data in order to investigate the limitations present when predicting retention properties using PSD data.

©xxxx NRC Canada

Draft

2. Soil skeleton approximations

2.1. Particle shape

As suction is determined by the shapes of menisci suspended between soil particles, it is important to consider particle shapes which can reproduce the retention properties of pores of varying sizes. A method to determine the suitability of an approximation to a particle shape is to consider the assumed particle's specific surface area (SSA). Figure 4 shows calculated SSA values for different particle sizes as compared to measured data, where the SSA of a spherical particle is calculated via

$$SSA_{sphere} = \frac{4\pi R^2}{\frac{4}{3}\pi R^3 \rho} = \frac{3}{\rho R} \tag{3}$$

where ρ is the particle density, assumed to be 2650 kg/m^3, and the range of values of R used is as given in Table 1. Although the spherical particle assumption closely matches those SSA values measured for larger particles ($\geq$ silts), Figure 4 shows that it fails to capture the higher SSA values of clay particles, so that suctions predicted for pores surrounded by these particles will suggestibly not be representative of the real material (Iwamatsu and Horii, 1996). Instead, images of clay particles, for example as shown in Figure 5, suggest that these particles might be more appropriately modelled as being cuboidal in shape. The SSA of such a cuboidal particle can be calculated using

$$SSA_{cuboid} = \frac{L^2(2+4\alpha)}{L^3\alpha\rho} = \frac{2(1+2\alpha)}{L\alpha\rho} \tag{4}$$

where L and α (the particle side length and height-to-length ratio respectively) are as given in Table 1 and are dependent on clay mineralogy. Note that these are the SSA values for individual particles only, i.e. no particle-particle contact area is considered. Figure 4 shows, by assuming that particles smaller than silts are cuboidal in shape, that a much closer approximation to measured SSA values is achieved for little increase in geometrical complexity. Note that, here, one value of α is used to describe clay particles of a given mineralogy. As clay particle arrangements are known to change with water content, however, it might be that a more appropriate representation of the clay particle structure can be achieved by having the value of α change with water content. However, as this would also result in a change in the pore size between the particles, a single value of α is considered here to enable measured PSDs to be used to directly determine retention properties for small pores. A variable value of α could,

©xxxx NRC Canada

Draft

however, be a topic for further study. Therefore, the assumption is made here that larger particles (silts and above) can successfully be modelled as spheres, as assumed by previous authors, and clay particles as cuboids. For convenience, pores surrounded by particles modelled as spheres are said to belong to the *macro region*, whilst those surrounded by cuboids belong to the *micro region*.

2.2. Particle arrangement

2.2.1. Macro region

As the volume of voids present within a soil determines the amount of water present at saturation, it is essential that soil particle geometry is modelled so that material porosity is maintained. This is not possible if it is assumed that all particles are in contact as the porosity is then set by the efficiency of the chosen packing regime. If, however, a separation distance D is specified between particle surfaces, as shown in Figure 6, then a range of material porosities n can be incorporated, as calculated via

$$n = 1 - \frac{4\sqrt{2\pi R^3}}{3\left(2R + D\right)^3} \tag{5}$$

where R is the particle radius. Note that a tetrahedral packing regime is used here, as opposed to the cubic regime used by previous authors, as the improved packing efficiency allows for a greater range of porosities to be modelled (cubic packing has a minimum porosity, i.e. where $D = 0$, of 0.476, whereas that of tetrahedral packing is 0.260). Another advantage of this approach is that, by setting $D > 0$, the effects of particle surface asperities, which would impede contact during packing, can also be incorporated, so that results for smooth-surfaced particles can be related to those for real, rough-surfaced materials (Molenkamp and Nazemi, 2003; Butt, 2008). As for previous models, it is assumed that menisci all reside between particles of equal size for a given pore size in order to maintain the simple packing geometries shown in Figure 6. Although a simplification, as menisci in real soils are likely to reside between dissimilarly-sized particles, an effective particle radius ($R^* = \frac{R_1 R_2}{R_1 + R_2}$ where R_1 and R_2 are the radii of the two subtending particles) must then be used to determine that meniscus' retention properties, so that, in effect, the calculation still considers menisci between equal-sized particles. Therefore, the assumption that menisci reside between equal-sized particles only is suggestibly justified.

©xxxx NRC Canada

Draft

Given the required porosity, interstitial pore size r can be found using

$$r = R\left(\frac{\sqrt{6}}{2} - 1\right) + \frac{\sqrt{6}}{4}D. \quad (6)$$

so that R and D can be solved for using Eqns 5 and 6, for a given value of r from the PSD. As a result of this approach, particle grading and porosity are linked via

$$V_s(R) = V_v(r)\left(\frac{1}{n} - 1\right) \quad (7)$$

where $V_s(R)$ is the volume of solids of particle size R and $V_v(r)$ is the volume of voids of radius r, so that the PSD and modelled particle grading are simple transformations of each other. It should be noted, however, that it is not the function of this model to accurately predict the material particle grading but rather to model an arrangement of particles surrounding the pores which give rise to similar retention properties as seen in real materials.

Pore interconnectivity is discussed in Haines (1929), who suggested that porous media contain two pore types, namely cavities and throats, with large cavities being separated and connected by the much narrower throats. This structure results in hysteresis between wetting and drying water contents on a change in suction, as drying is controlled by the emptying of the narrow throats (i.e. at high suctions), whereas wetting is controlled by the filling of the larger cavities (i.e. at lower suctions) (Everett, 1967; Rojas et al., 2010). However, by considering pores to be in isolation, hysteresis of the wetting and drying retention properties can no longer be considered in this manner. This is a necessary simplification, however, as the modelling of a connected pore network would be computationally unfeasible. Instead, hysteresis is introduced by considering different wetting and drying mechanisms, based solely on the modelled geometry of the individual pore; these mechanisms will be discussed in the following sections.

Draft

2.2.2. Micro region

Cuboid particles are assumed to be stacked one on top of the other, with pore spaces in between, so that the unit cell comprises a single pore flanked by two particles of half width (i.e. $\frac{\alpha L}{2}$) as shown in Figure 7. Therefore, the porosity of the micro region is controlled by mineralogy only. Although this might be considered a shortfall of the model, porosity is a global value and is not representative of the

©xxxx NRC Canada

void ratio at different scales (i.e. local fluctuations are not considered). The lack of a consideration of porosity in the micro region is therefore arguably justifiable when considering overall material retention properties

3. Main drying path calculations

3.1. Cavitation

Water under an applied suction is in a metastable state, in that it remains in liquid form despite pressures being lower than its vapour pressure (Or and Tuller, 2002). Cavitation is the process of the formation and subsequent expansion of vapour bubbles within a liquid on a change in liquid pressure (Young, 1989). Homogeneous cavitation (also called homogeneous nucleation) is the formation of cavities (bubbles) of pure liquid vapour in the surrounding liquid. If it is assumed that random thermal motion of the water molecules leads to the formation of a spherical cavity between them of a diameter equal to the minimum distance between water molecules in liquid water (0.35 nm), then the subsequent liquid pressure required for equilibrium can be found using Eqn 1:

$$u_w = u_a - \frac{2\gamma}{\kappa} = 2.3 \text{ kPa} - \frac{0.1454}{0.175 \times 10^{-6}} = -830.6 \text{ MPa} \tag{8}$$

where γ has been calculated using $\gamma = 0.1171 - 0.0001516T$, where T is the absolute temperature, set to 293 K, and $u_a = 2.3$kPa is the vapour pressure of water at 293 K (Edlefsen and Anderson, 1943; Marinho et al., 2008). This suction value, however, is rarely achieved in experiments due to heterogeneous cavitation, namely the formation of bubbles of dissolved gas which vaporises at significantly lower suctions. Cavitation of liquids containing dissolved gases was discussed in Or and Tuller (2002), who suggested that the energy required (ΔE) to form a bubble of radius r in a liquid can be calculated from the sum of the interfacial energy of the bubble surface and the opposing work done by the fluid on the volume of the resulting bubble according to

$$\Delta E = 4\pi r^2 \gamma - \frac{4\pi}{3} r^3 \psi, \tag{9}$$

©xxxx NRC Canada

which has a minimum at

$$\frac{\partial \Delta E}{\partial r} = r^{\star} = \frac{2\gamma}{\psi}, \tag{10}$$

so that $r^{\star}$ is the minimum bubble radius required in order for the creation of a bubble to be energetically favourable and ψ is the corresponding cavitation suction. The pressure equilibrium between the gas in the bubble and the surrounding fluid can then be determined via the Kelvin equation

$$\psi = \frac{R_u T}{v_m} \log\left(\frac{p}{p^{\star}}\right) \tag{11}$$

where R_u is the universal gas constant (8.314 Jmol^{-1}K^{-1}), v_m is the specific molar volume of the fluid (m^{3}kg^{-1}mol^{-1}) and p and $p^{\star}$ are the vapour pressure and saturated vapour pressure (i.e. that under free conditions) of the fluid in the gas respectively. It follows from Eqn 10 that pores smaller than $r^{\star}(\psi)$ must remain filled for that value of ψ, as bubbles of sufficient size for the mechanism to be energetically favourable cannot form. An example of this is shown in Figure 8 for a range of pore sizes, where suction increases from Figure 8(a) to Figure 8(c). An advantage of the use of a cavitation mechanism is that it does not require a continuous water phase in order to be valid, as it arises due to an air-water interface only (i.e. suction is continuous and uniform in a discontinuous (but static) water phase) (Or and Tuller, 2002). Therefore, it is compatible with the modelling of pores in isolation, as discussed in the previous section.

Attraction between water molecules and particles results in a film of adsorbed water being developed on particle surfaces, as previously discussed. The thickness of an adsorbed film, t, on a single, isolated surface is given by

$$t = \sqrt[3]{\frac{A_{svl}}{6\pi(\rho_l - \rho_v)\Delta\mu}} \tag{12}$$

where $A_{svl} = -6 \times 10^{-20}$J is the Hamaker constant for solid-vapour interactions through an intervening liquid, ρ_l and ρ_v are the liquid and vapour densities respectively and $\Delta\mu$ is the change in chemical potential (μ) associated with a change in vapour pressure, which can be calculated via

$$\Delta\mu = kT \log\left(\frac{p}{p^{\star}}\right) \tag{13}$$

©xxxx NRC Canada

Draft

where k is Boltzman's constant (Iwamatsu and Horii, 1996). The value of $A_{svl} = -6 \times 10^{-20}$J has been selected following the work of Or and Tuller (1999), who suggested that such a value is suitable for adsorption in soils containing mixed clays, although it should be noted that this value generally varies between -10^{-19} and -10^{-20} depending on soil mineralogy (Frydman and Baker, 2009). Given that k is related to R_u via

$$k = \frac{R_u}{N_A} \tag{14}$$

where N_A is the Avogadro constant and that $\Delta\mu$ is related to ψ via

$$\Delta\mu = \frac{\psi}{\rho}, \tag{15}$$

Eqns 14 and 15 can be substituted into Eqn 13 to give

$$\psi = \frac{R_u T}{v_m} \log\left(\frac{p}{p^\star}\right) \tag{16}$$

i.e. Eqn 11 as before (Tuller et al., 1999). Therefore, given that $\rho_l \gg \rho_v$, adsorbed film thickness can be related to the suction present in the fluid via

$$t(\psi) \approx \sqrt[3]{\frac{-A_{svl}}{6\pi\psi}}. \tag{17}$$

Eqn 17 can be used to determine the thickness of an adsorbed film on the surface of a spherical particle provided $t \ll R$ (Tuller et al., 1999; Likos, 2009). Given the presence of this film, the minimum cavitation radius $r^\star$ in a pore of radius r must therefore be modified as shown in Figure 9 to incorporate that water surrounding the pore space which cannot cavitate (as it is bound to the particle surface), according to

$$r^\star = r - t(\psi) \tag{18}$$

so that the cavitation suction ψ for that pore size r can then be found using Eqn 10 (Shull, 1948; Collet et al., 2008).

©xxxx NRC Canada

Draft

Although it is assumed above that adsorbed water is in the form of thin films covering particle surfaces, it was shown in Lourenço et al. (2012) that water instead exists on the surface of rough granular particles in the form of droplets. Results presented in Lourenço et al. (2012) also suggest, however, that successive wetting and drying cycles result in a coalescence of these surface droplets, so that they progressively become more film-like. As it is assumed here that materials are first dried from a saturated state, it is therefore likely that water will remain in continuous films on particle surfaces rather than as discontinuous bodies, so that the use of films to represent adsorbed water is suggestibly justified. However, the effect of surface droplets on the retention properties of granular particles and methods to predict their shapes is an interesting topic of ongoing research.

Draft

3.2. Cavitation and adsorption in slit-shaped pores

A water meniscus trapped between two cuboidal particles is shown in Figure 7 and in more detail in Figure 11. The thickness of adsorbed water films in a slit-shaped pore, t_{ss}, at a given suction ψ is given by

$$\psi = -\frac{A_{svl}}{6\pi\left(2r - t_{ss}(\psi)\right)^3} + \frac{A_{llv}}{48\pi\left(r - t_{ss}(\psi)\right)^3} - \frac{A_{svl}}{6\pi t_{ss}(\psi)^3} \tag{19}$$

where r is the pore radius (given by the PSD) and $A_{llv} = 3.7 \times 10^{-20}$J is the Hamaker constant for liquid-liquid interactions through an intervening vapour (Iwamatsu and Horii, 1996). Note that Eqn 19 has been converted from the original expression given in Iwamatsu and Horii (1996) to be in terms of ψ, as discussed in the previous section. The suction required to cavitate the pore is given by Eqns 10 and 18 as

$$\psi = \frac{2\gamma}{r^\star} = \frac{2\gamma}{\left(r - t_{ss}(\psi)\right)} \tag{20}$$

so that Eqns 19 and 20 can be solved to find $t_{ss}(\psi)$ and so ψ. Films of thickness $t_{ss}(\psi)$ remain adsorbed to the surfaces of the slit-shaped pore after the pore has cavitated (Shull, 1948).

©xxxx NRC Canada

4. Main wetting path calculations

4.1. Liquid bridges

Cavitation of the water contained within a pore results in the formation of menisci, often referred to as *liquid bridges* due to their shape, suspended between the surrounding soil particles. On re-wetting, those liquid bridges expand up to the point that their boundaries touch, whereupon the pore fills with water (Likos, 2009). Suction in the liquid bridges is given by Eqn 2, where κ and l are the meridional and azimuthal radii given by

$$\kappa = \frac{2R_{mod}\left(1-\cos\left(\beta\right)\right)+D_{mod}}{2\cos\left(\theta_{slv}+\beta\right)} \tag{21}$$

$$l = R_{mod}\sin\left(\beta\right)-\kappa\left(1-\sin\left(\theta_{slv}+\beta\right)\right) \tag{22}$$

where $R_{mod}=R+t(\psi_w)$, $D_{mod}=D-2t(\psi_w)$ ($t(\psi_w)$ is found using Eqn 17) and β is the filling angle, as shown in Figure 12. Suction in the liquid bridge given by Eqn 2 is now termed ψ_w as it is to be used to determine wetting suctions. At the moment of cavitation, suction in the liquid bridge is equal to the cavitation suction ψ as calculated using Eqn 10, so that it can readily be shown from Eqns 17, 18, 10 and 2 that $\kappa < r^{\star}$, as shown in Figure 13(a) for cubically-packed spheres (for ease of demonstration). A reduction in suction immediately following cavitation therefore does not result in the immediate filling of the pore space, as individual liquid bridges are not in contact, but instead a gradual growth in liquid bridge volume with reducing suction until the point at which they coalesce. Liquid bridge coalescence occurs at $\beta = 30°$ for tetrahedrally-packed spheres, assuming that $\theta_{slv}=0$, so that the suction at coalescence can be found for a given value of r, R and D using Eqn 2 (Likos, 2009). It should be noted that $\theta_{slv}=0$ for wetting and drying due to the presence of adsorbed films on the smooth particle surfaces, which are therefore perfectly wetting (Lourenço et al., 2012). Hysteresis between wetting and drying suctions is often attributed to different wetting and drying θ_{slv} values, due to assumed "advancing" and "retreating" conditions respectively (Haines, 1929, 1930; Lourenço et al., 2012); however, by incorporating different mechanisms for wetting and drying (i.e. meniscus coalescence and cavitation respectively), this model is therefore also able to include suction hysteresis despite the $\theta_{slv}=0$ restriction.

If $D > 0$, it is possible that $\kappa \geq l$ for some values of β, as shown in Figure 14. This condition is undefined, as the geometry shown in Figure 12 cannot be maintained. It is therefore assumed that

©xxxx NRC Canada

Draft

if the condition $\kappa \geq l$ is met for a given pore size, the liquid bridges surrounding that pore rupture, so that only adsorbed water remains. $\kappa \geq l$ is also possible if too high a value of n is selected, as this results in high values of D and so a 'stretching' of the liquid bridge geometry. The maximum porosity that can be supported by the assumed tetrahedral geometry can be determined by setting $\kappa = l$ and solving between Eqns 21, 22 and 5, resulting in $n_{max} = 0.519$, so that materials of porosities $0.276 \leq n \leq 0.519$ can be modelled using tetrahedral packing.

4.2. Filling of slit-shaped pores

The suction below which a slit-shaped pore will fill is given by

$$\psi_w = -\frac{1}{2(r - t(\psi_w))}\left(\frac{A_{svl}}{6\pi t(\psi_w)^2} + \frac{A_{llv}}{48\pi\left(r - t(\psi_w)\right)^2} - \frac{A_{svl}}{6\pi\left(2r - t(\psi_w)\right)^2} - 2\gamma\right) \tag{23}$$

where $t(\psi_w)$ is found using Eqn 17 (as bulk and adsorbed water phases are not interacting, so that Eqn 19 is not required). Again, Eqn 23 has been converted from the original Iwamatsu and Horii (1996) expression to be in terms of ψ_w.

5. Water content calculations

5.1. Drying of macro-region pores

Pores between spherical particles are either filled or occupied by adsorbed films and liquid bridges (unless they have ruptured), depending on the applied suction and pore size. The volume of water in filled pores of size r can be found directly from the soil PSD, given by the cumulative volume of pores of that size. The volume of water contained in a liquid bridge immediately following cavitation, V_{LB}, is given by

$$V_{LB} = \pi R^*_{mod}\left(4\kappa^2 c^2 - \left(D_{mod} - 2t(\psi(r))\right)^2\right) \tag{24}$$

$$c = \frac{\cos(\theta + \beta) + \cos\theta}{2} \tag{25}$$

where $R^*_{mod} = \dfrac{R_{mod}}{2}$ and $t(\psi(r))$ is as found using Eqn 17. β, κ and l are found using Eqns 2, 21 and 22 for a given value of $\psi(r)$. Note that although Eqns 24 and 25 refer to liquid bridges, the cavitation suction ψ and not the coalescence suction ψ_w is used for volume determination in this case as conditions are for drying. Cavitation leads to the formation of $\left(6 \times \frac{1}{2}\right) + \left(6 \times \frac{1}{4}\right) + 9 = 27$ liquid

©xxxx NRC Canada

bridges in the enlarged tetrahedral cell (Figure 6), so that the volume of water contained within the liquid bridges, expressed as the ratio of water volume in the liquid bridges, $V_{LB_{cell}}$, to volume of voids in the cell, $V_{v_{cell}}$, is given by

$$\frac{V_{LB_{cell}}}{V_{v_{cell}}}_{tet} = \frac{27V_{LB}}{\left(3\sqrt{2}\left(2R+D\right)^3 - 8\pi R^3\right)}. \tag{26}$$

Note that R_{mod} and D_{mod} are not required in Eqn 26 due to the use of the volume of voids for the total unit cell. The corresponding water content for liquid bridges surrounding all pores of size r is therefore given by

$$V_{LB_r} = v_p(r)\left(\frac{V_{LB_{cell}}}{V_{v_{cell}}}\right) \tag{27}$$

where $v_p(r)$ is the volume of pores of size r, found from the soil PSD.

As liquid bridges can be present above the cavitation suction, the total volume of water contained within all liquid bridges, $V_{T_{LB}}$, is found by summing V_{LB_r} over all pore sizes $\geq r$, all determined at suction $\psi(r)$ (i.e. the currently-considered cavitation suction), noting that V_{LB_r} can equal 0 if the applied suction is too high for that pore geometry (i.e. the liquid bridges have ruptured).

The volume of water contained in an adsorbed film surrounding a particle of radius R is given by

$$V_{film} = 4\pi R^2 t(\psi(r)). \tag{28}$$

The total surface area for adsorption is $\left(12\times\frac{1}{6}\right)+\left(2\times\frac{1}{2}\right)+3=6$ spheres in the expanded tetrahedral unit cell, so that the total volume of adsorbed water in the unit cell expressed as the ratio of water volume in the adsorbed films $V_{film_{cell}}$ to volume of voids is given by

$$\frac{V_{film_{cell}}}{V_{v_{cell}}}_{tet} = \frac{6V_{film}}{\left(3\sqrt{2}\left(2R+D\right)^3 - 8\pi R^3\right)} \tag{29}$$

so that

$$V_{film_r} = v_p(r)\left(\frac{V_{film_{cell}}}{V_{v_{cell}}}\right) \tag{30}$$

©xxxx NRC Canada

gives the adsorbed water content for all pores of that pore radius. Again, the total volume of water contained within adsorbed films, $V_{T_{film}}$, is given by the sum of V_{film_r} over pore sizes $\geq r$. The total volume of water present in the soil at a given drying suction ψ is therefore given by

$$\mathrm{V}_T = \sum_{<r} v_p(r) + V_{T_{LB}} + V_{T_{film}} \tag{31}$$

5.2. Drying of micro-region pores

It is assumed that slit-shaped pores of size r remain filled at suctions below $\psi(r)$, so that the water content of filled pores is again given by $v_p(r)$. The total volume of water remaining in a slit-shaped pore of size r after cavitation is given by

$$V_{ss_r} = v_p(r)\frac{t_{ss}(\psi)}{r} \tag{32}$$

where t_{ss} is found using Eqn 19 for that suction ψ. Note that the particle length L and height αL do not feature in Eqn 32, as the assumption that pores are rectangular in cross section results in pore water content being determined by the ratio of film thickness to pore radius only. The total volume of water contained within adsorbed films between slit-shaped pores, $V_{T_{ss}}$, is given by the sum of V_{ss_r} over all pores $\geq r$. The total volume of water at a given suction ψ, considering cavitation of the slit-shaped pores, is therefore given by

$$\mathrm{V}_T = \sum_{<r} v_p(r) + V_{T_{LB}} + V_{T_{film}} + V_{T_{ss}} \tag{33}$$

5.3. Wetting calculations

The total volume of water present in the macro region during wetting is calculated using Eqns 24 to 27 at $\psi_w(r)$, determined using to Eqn 2. The total water content is then given by

$$\mathrm{V}_T = \sum_{\leq r} v_p(r) + V_{T_{LB}} + V_{T_{film}} \tag{34}$$

i.e. as for Eqn 31, however now pores are considered to be filled at ψ_w. As $\psi_w(r) < \psi(r)$, the volume of water on wetting is lower than that during drying, as pores can maintain liquid bridges to lower suctions, so that hysteresis is expected between the filling and emptying.

©xxxx NRC Canada

Draft

Similarly, the total volume of water present in the micro region is calculated using Eqns 25 to 27 and Eqn 32 at $\psi_w(r)$ for slit-shaped pores. Total water content during wetting is then given by

$$\mathrm{V}_T = \sum_{\leq r} v_p(r) + V_{T_{LB}} + V_{T_{film}} + V_{T_{ss}}. \tag{35}$$

Again, this results in a lower volume of water due to lower wetting than drying suctions for slit-shaped pores. A summary of all of the model calculations is given in Figure 15.

6. Model performance and discussion

6.1. SWRC prediction

SWRCs for five colluvial soils formed from a naturally decomposed granitic soil were presented in Zhang and Li (2010), as well as corresponding PSDs for those soils under zero applied suction as shown in Figure 16. Mercury Intrusion Porosimetry (MIP) was used to determine soil PSDs using freeze-dried samples (Penumadu and Dean, 2000). Material was as used for SWRC analysis, but was sieved to pass 10 mm due to the size limit on MIP samples (15 cm^3 for the device used). Modified and original particle grading curves for each soil are shown in Figure 17, indicating that whilst the grading of soil CL was unchanged by this process, the grading of the remaining soils changed considerably due to particle removal. Compacted densities were modified to account for the removed material, so that the final densities of the MIP and SWRC test samples, and so their resulting pore structures, were comparable. A disadvantage of the use of MIP to determine PSDs is that the range of pore sizes accessible is dependent on the pressure range of the apparatus. PSDs found by Zhang and Li (2010) for compacted and saturated samples (selected as this is the starting condition for experimental SWRC analysis) identified pore diameters between 6 nm and 146 μm and results suggest that no pores smaller than 6 nm were present in any of the samples, which is consistent with the larger pores expected in kaolinitic clays (Diamond, 1970). Only soil GW-GM showed a significant volume of pores larger than 146 μm.

SWRCs predicted from those PSDs shown in Figure 16 are shown in Figures 18 to 22. A summary of the model input and output data (for the main drying curves only) is given in Table 2. Approximations to the SWRC made using Eqn 1 (which are identical to those predicted in Zhang and Li (2010)) are also shown in Figures 18 to 22, showing that, whilst similar, the model developed here predicts

©xxxx NRC Canada

Draft

higher suctions for a given water content; this is due to the effective reduction in pore size due to the presence of adsorbed films, as shown by Eqn 18. Note that although it is usual to show SWRCs in terms of degree of saturation, it is not possible in this case due to the use of different sample sizes between SWRC and PSD testing; the use of gravimetric water content removes this restriction. Figures 18 to 22 also show predicted main wetting curves and adsorbed water contents for each PSD shown in Figure 16. Unfortunately, PSDs were not determined in Zhang and Li (2010) for wetting conditions, so that those main wetting curves shown in Figures 18 to 22, calculated using drying PSDs, are illustrative of the model's ability to predict hysteresis between drying and wetting only. Similarly, adsorbed water contents were not measured in Zhang and Li (2010), so that those adsorbed water contents shown are also only indicative of how adsorbed water content might change with overall water content and suction. Confirmation of predicted wetting retention properties and adsorbed water contents is a topic of ongoing study.

Figures 18 to 22 indicate that the best match to measured data was achieved for soil CL; this is suggestibly due to the use of identical material during SWRC and PSD testing, as shown in Figure 17, unlike those used for the other soil types. However, they also show that predicted values all show a characteristic overshoot in the low suction range, where significantly higher suctions are predicted for given water contents than were found experimentally. The exception to this is soil GW-GM (Figure 19), which shows a good match between predicted and measured data in the low suction range but a poorer match at higher suctions; this is likely due to the significant volume of pores larger than 146 μm which could not be measured using the selected MIP device (Zhang and Li, 2010).

A potential source of the apparent overshoot is "pore trapping", which occurs when pores of different radii lie on the mercury intrusion path and which has also been suggested as a contributing factor towards hysteresis observed between drying and wetting retention properties (Cuisinier and Laloui, 2004; Rojas and Rojas, 2005). An example columnar pore is shown in Figure 23. If mercury intrudes the from the left, the larger pore region (radius r_1) will fill at some suction $\psi(r_1)$ and the smaller region (radius $r_2 < r_1$) at a higher suction $\psi(r_2)$, with the change in the intruded volume of mercury being attributed to pores of sizes r_1 and r_2 respectively. However, if mercury intrudes from the right the larger region cannot be filled due to the higher intrusion pressure of the smaller region. Instead, both regions are intruded at $\psi(r_2)$, with the change in the intruded volume for both regions being attributed to pores of size r_2 only (Simms and Yanful, 2001). The effect of trapped pores on MIP results

©xxxx NRC Canada

is therefore an underestimation of the volume fraction of larger pores and a subsequent overestimation of that of smaller pores, resulting in higher and lower water contents for a predicted drying suction respectively, as is seen in Figures 18 to 22 (Meyer and Klobes, 1999). Pore trapping could therefore be responsible for the characteristic overshoot seen in Figures 18 to 22 and so demonstrates the need to use multiple methods to determine soil PSDs, in order to minimise the impact of one single test on measured results (Hajnos et al., 2006).

6.2. Soil fabric evolution and SWRC prediction limitations

The effect of changing suction on the fabric of double-structure soils has been investigated by several authors. Simms and Yanful (2001) used MIP to measure the PSDs of freeze-dried samples of a clayey glacial till (compacted wet of optimum) after the application of a suction and found that, with increasing suction, void ratio decreased and the modal large pore size and volume reduced, whilst the small pore mode remained at a constant size but grew in volume. The change in PSD with suction was attributed to the constriction of larger soil pores and so a reduction in pore accessibility with increasing suction.

Cuisinier and Laloui (2004) used a pressure plate to subject samples of a morainic sandy-loam soil (compacted on the dry side of optimum) to successively increasing suction levels to determine the effect of suction on soil fabric. Material was removed from the samples on reaching suction equilibrium and freeze-dried so that PSDs could be determined using MIP as shown in Figure 24. As was found by Simms and Yanful (2001), increasing suction resulted in a reduction in the volume of large pores, with the large pore modal size decreasing slightly with increasing suction, and an increase in the volume of smaller pores, again with no significant change in the small pore modal size. Soil void ratio again reduced with increasing suction although changes in soil PSD occurred at near-constant void ratios at higher suctions. Cuisinier and Laloui (2004), and later Tarantino (2010), suggested that observed results were due to the application of suctions only high enough to drain the larger pores, so that only larger pores were subjected to changes in water content and subsequently constricted, whilst smaller pores remained filled at all suction levels tested.

Results found by these authors therefore show that the fabric of a soil changes whilst undergoing SWRC testing, so that retention properties predicted from one PSD alone, as was done in the previous section, cannot capture the material behaviour at different suction levels. Instead, a single PSD can

©xxxx NRC Canada

Draft

only reliably predict material retention properties at the suction value at which it was found, so that numerous PSDs are required to determine a more complete SWRC (Nuth and Laloui, 2008). This can be investigated by comparing measured SWRC values to predictions made using a succession of PSDs, determined over a range of suction values, a shown in Figure 25 for PSDs given in Figure 24. Although the model considers particles to be rigidly arranged for purposes of the analysis, the use of a different PSD per suction level prediction accounts for a changing (i.e. non-rigid) particle structure. Figure 25 shows that although predictions made using a single PSD do not capture the measured retention properties, a good match to predicted data can be achieved by combining predictions for each PSD for that PSD's suction level. The large difference between measured and predicted water contents shown in Figure 25 is due to the significant difference between the saturated water content found for SWRC testing (370 mL/g) and the maximum intruded volume of mercury found at zero suction (305 mL/g), suggestibly due to a large volume of pores not being intruded during MIP testing, either due to the limit on intrusion pressures inherent in the device or pores not being accessible to mercury during testing (Cuisinier and Laloui, 2004; Koliji et al., 2006). Also given in Figure 25 are results found using Eqn 1, again showing how Eqn 1 significantly underpredicts suction values for a given water content. Results given in Figure 25 therefore show that a good approximation to measured SWRC data can be achieved by this model through the use of multiple PSDs, determined over a range of applied suctions. This result unfortunately diminishes the power of the use of soil PSDs for predicting retention properties, however, as a large number of PSDs is therefore required in order to get a good match to experimental data. The use of PSDs to predict retention properties nonetheless remains a powerful tool, but predictions must be limited to those suction values investigated.

7. Conclusions

This paper has presented a new method for determining a material's retention properties from its PSD and has discussed the limitations on the use of PSDs to predict retention properties.

The model presented here offers several advantages over those techniques used by previous authors:

- Particles are modelled either as spheres or cuboids in order to more accurately model retention properties at different pore scales;
- Material porosity, determined from the material PSD, is included as a model variable, incorpo-

©xxxx NRC Canada

rated by assuming a finite separation distance between modelled particles;

- The effects of adsorbed water on both wetting and drying suctions are included by assuming that particles are covered by thin adsorbed films, with a subsequent improvement to the accuracy of predicted retention properties;

- Cavitation and liquid coalescence are used as mechanisms to explain pore drainage and filling respectively, which allows the model to predict hysteresis between drying and wetting conditions in the presence of adsorbed films without the need to consider the effects of pore interconnectivity.

The effect of changing suction on soil fabric was discussed and it was shown that the match to experimental data is significantly improved if predictions are made using PSDs determined over a range of suction values. This result unfortunately diminishes the power of the ability to predict retention properties using PSD data, as multiple PSDs, determined for the entirety of the suction range of interest, are required. Although currently a time-consuming process, developments in non-destructive testing equipment, for example X-Ray Computed Tomography, might improve the speed of PSD determination to the point that retention property prediction from PSD data becomes viable. Regardless, the use of PSDs to predict retention properties has been shown to be a useful and accurate alternative to direct SWRC measurement provided suitable PSDs are available.

8. Acknowledgements

The first author was supported by a studentship awarded by the School of Engineering and Computing Sciences, Durham University, during this research. The first author would like to thank Profs. Alessandro Tarantino and David Toll for their comments on this work.

©xxxx NRC Canada

Draft

References

Abdullah, W. S., Alshibli, K. A., Al-Zou'bi, M. S., 1999. Influence of pore water chemistry on the swelling behavior of compacted clays. Applied Clay Science 15 (5-6), 447–462.

Akbour, R. A., Douch, J., Hamdani, M., Schmitz, P., Sep 2002. Transport of kaolinite colloids through quartz sand: Influence of humic acid, ca2+, and trace metals. Journal of Colloid and Interface Science 253 (1), 1–8.

Baker, R., Frydman, S., 2009. Unsaturated soil mechanics: Critical review of physical foundations. Engineering Geology 106 (1-2), 26–39.

Butt, H.-J., 2008. Capillary forces: Influence of roughness and heterogeneity. Langmuir 24 (9), 4715–4721.

Choquette, M., Brub, M.-A., Locat, J., 1987. Mineralogical and microtextural changes associated with lime stabilization of marine clays from eastern canada. Applied Clay Science 2 (3), 215–232.

Collet, F., Bart, M., Serres, L., Miriel, J., 2008. Porous structure and water vapour sorption of hemp-based materials. Construction and Building Materials 22 (6), 1271–1280.

Cosenza, P., Tabbagh, A., 2004. Electromagnetic determination of clay water content: role of the microporosity. Applied Clay Science 26, 21–36.

Cuisinier, O., Laloui, L., 2004. Fabric evolution during hydromechanical loading of a compacted silt. International Journal for Numerical and Analytical Methods in Geomechanics 28 (6), 483–499.

Derjaguin, B. V., Churaev, N. V., , Muller, V. M., 1987. Surface forces. Plenum, New York (USA).

Diamond, S., 1970. Pore size distribution in clays. Clays and Clay Minerals 18, 7–23.

Edlefsen, N. E., Anderson, A. B. C., 1943. The thermodynamics of soil moisture. Hilgardia 16, 31–299.

Everett, D. H., 1967. The solid—gas interface. Dekker, New York (USA).

Frydman, S., Baker, R., 2009. Theoretical soil-water characteristic curves based on adsorption, cavitation, and a double porosity model. Int. J. Geomech. 9 (6), 250–257.

Gens, A., 2010. Soil-environment interactions in geotechnical engineering. Géotechnique 60 (1), 3–74.

©xxxx NRC Canada

Draft

Ghanbarian-Alavijeh, B., Liaghat, A. M., 2009. Evaluation of soil texture data for estimating soil water retention curve. Canadian Journal of Soil Science 89 (4), 461–471.

Grof, Z., Lawrence, C. J., Stepnek, F., 2008. The strength of liquid bridges in random granular materials. Journal of Colloid and Interface Science 319 (1), 182–192.

Haines, W. B., 1929. The hysteresis effect in capillary properties and the mode of moisture distribution associated therewith. Journal of Agricultural Science 20 (7).

Haines, W. B., 1930. Studies in the physical properties of soil. v. the hysteresis effect in capillary properties, and the modes of moisture distribution associated therewith. The Journal of Agricultural Science 20 (01), 97–116.

Hajnos, M., Lipiec, J., Swieboda, R., Sokolowska, Z., Witkowska-Walczak, B., 2006. Complete characterization of pore size distribution of tilled and orchard soil using water retention curve, mercury porosimetry, nitrogen adsorption, and water desorption methods. Geoderma 135, 307–314, doi: DOI: 10.1016/j.geoderma.2006.01.010.

Iwamatsu, M., Horii, K., 1996. Capillary condensation and adhesion of two wetter surfaces. Journal of Colloid and Interface Science 182 (2), 400–406.

Koliji, A., Laloui, L., Cusinier, O., Vulliet, L., Aug 2006. Suction induced effects on the fabric of a structured soil. Transport in Porous Media 64 (2), 261–278.

Likos, W. J., Jul 13-17 2009. Pore-scale model for water retention in unsaturated sand. Amer Inst Physics, Golden, CO, pp. 907–910.

Lourenço, S. D. N., Gallipoli, D., Augarde, C. E., Toll, D. G., Fisher, P., Congreve, A., 2012. Formation and evolution of water menisci at contacts in unsaturated granular media. Géotechnique 62 (3), 193–199.

Lu, N., Likos, W. J., 2004. Unsaturated Soil Mechanics. John Wiley & Sons, Inc., New Jersey (USA).

Marinho, F., Take, W., Tarantino, A., 2008. Measurement of matric suction using tensiometric and axis translation techniques. Geotechnical and Geological Engineering 26, 615–631.

©xxxx NRC Canada

Draft

Mayer, R. P., Stowe, R. A., 2006. Packed uniform sphere model for solids: Interstitial access opening sizes and pressure deficiencies for wetting liquids with comparison to reported experimental results. Journal of Colloid and Interface Science 294 (1), 139–150.

Meyer, K., Klobes, P., 1999. Comparison between different presentations of pore size distribution in porous materials. Fresenius' Journal of Analytical Chemistry 363 (2), 174–178.

Millington, R. J., Quirk, J. P., 1961. Permeability of porous media. Nature 183, 387–388.

Molenkamp, F., Nazemi, A. H., 2003. Interactions between two rough spheres, water bridge and water vapour. Géotechnique 53 (2), 255–264, times Cited: 12.

Mualem, Y., 1976. A new model for predicting the hydraulic conductivity of unsaturated porous media. Water Resour. Res. 12, 513–522.

Nuth, M., Laloui, L., 2008. Advances in modelling hysteretic water retention curve in deformable soils. Computers and Geotechnics 35 (6), 835–844.

Or, D., Tuller, M., 1999. Liquid retention and interfacial area in variably saturated porous media: Upscaling from single-pore to sample-scale model. Water Resour. Res. 35, 3591–3605.

Or, D., Tuller, M., 2002. Cavitation during desaturation of porous media under tension. Water Resour. Res. 38, 19–1–19–4.

Penumadu, D., Dean, J., 2000. Compressibility effect in evaluating the pore-size distribution of kaolin clay using mercury intrusion porosimetry. Canadian Geotechnical Journal 37, 393–405.

Philip, J. R., 1977. Unitary approach to capillary condensation and adsorption. Journal of Chemical Physics 66, 5069–5075.

Powrie, W., 2008. Soil Mechanics: Concepts and Applications, 2nd Edition. Spon Press.

Rojas, E., Gallegos, G., Leal, J., September 2010. A porous model based on porosimetry to simulate retention curves. In: Alonso, E., Gens, A. (Eds.), Unsaturated Soils. Fifth International Conference on Unsaturated Soils, CRC Press, pp. 927–932.

Rojas, E., Rojas, F., 2005. Modeling hysteresis of the soil-water characteristic curve. Soils and Foundations 45 (3), 135–145.

©xxxx NRC Canada

Draft

Shull, C. G., 1948. The determination of pore size distribution from gas adsorption data. Journal of the American Chemical Society 70 (4), 1405–1410.

Simms, P. H., Yanful, E. K., 2001. Measurement and estimation of pore shrinkage and pore measurement in a clayey till during soil-water characteristic curve tests. Canadian Geotechnical Journal 38, 741–754.

Stevens, N., Ralston, J., Sedev, R., 2009. The uniform capillary model for packed beds and particle wettability. Journal of Colloid and Interface Science 337 (1), 162–169.

Tang, A.-M., Cui, Y.-J., 2005. Controlling suction by the vapour equilibrium technique at different temperatures and its application in determining the water retention properties of MX80 clay. Canadian Geotechnical Journal 42 (1), 287–296.

Tarantino, A., 2010. Unsaturated soils: compaction versus reconstituted states. In: Alonso, E., Gens, A. (Eds.), Unsaturated soils. Fifth International Confernce on Unsaturated Soils, CRC Press, pp. 113–136.

Tuller, M., Or, D., 2004. Retention of water in soil and the soil water characteristic curve. In: Hillel, D. (Ed.), Encyclopedia of Soils in the Environment. Vol. 4. Elsevier Ltd., Oxford, U.K., pp. 278–289.

Tuller, M., Or, D., Dudley, L. M., 1999. Adsorption and capillary condensation in porous media: Liquid retention and interfacial configurations in angular pores. Water Resour. Res. 35 (7), 1949–1964.

Yong, R. N., Ouhadi, V. R., 2007. Experimental study on instability of bases on natural and lime/cement-stabilized clayey soils. Applied Clay Science 35 (3-4), 238–249.

Young, F. R., 1989. Cavitation. McGraw-Hill Book Company (UK) Ltd.

Zhang, L. M., Li, X., 2010. Microporosity structure of coarse granular soils. J. Geotech. and Geoenvir. Engrg. 136 (10), 1425–1436.

Draft

©xxxx NRC Canada

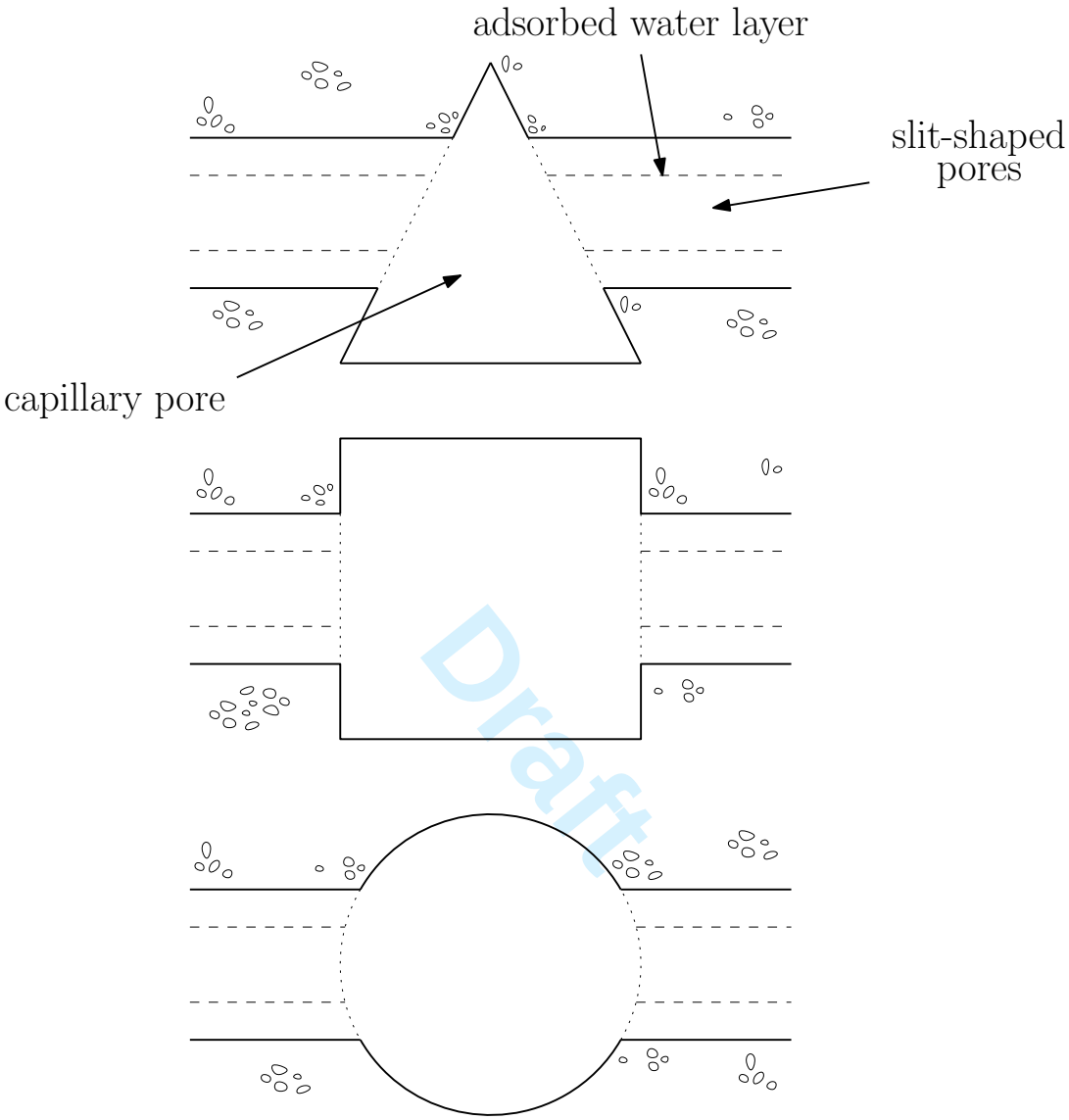

Fig. 1. Examples of pore shapes considered in Tuller et al. (1999), showing decreasing angularity

Draft

©xxxx NRC Canada

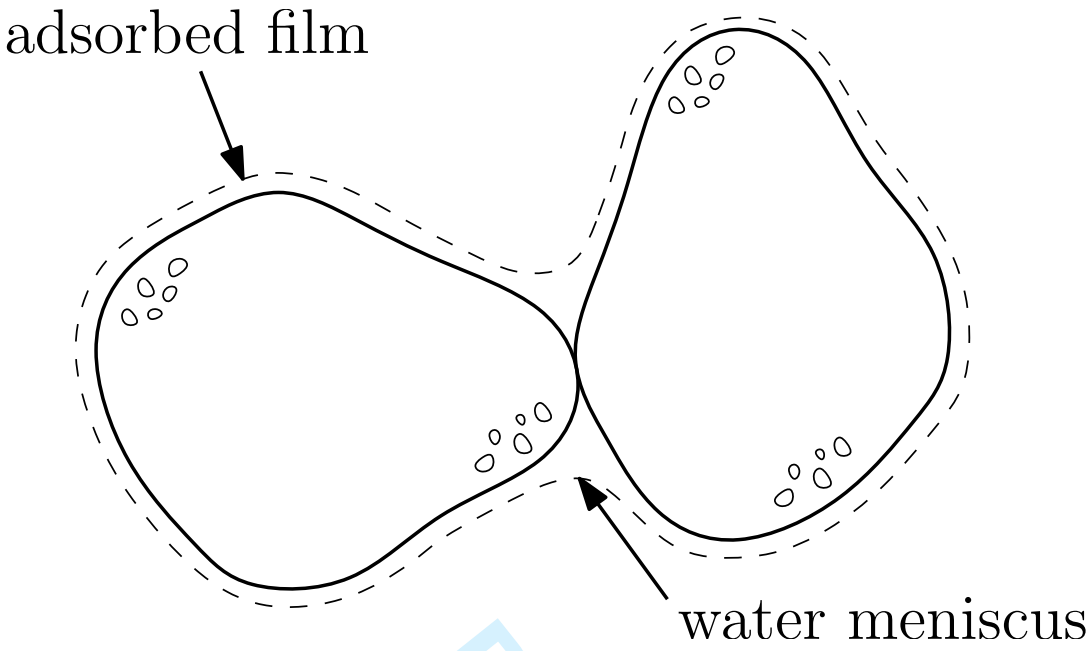

Fig. 2. Water meniscus and adsorbed films between two example granular particles

Draft

©xxxx NRC Canada

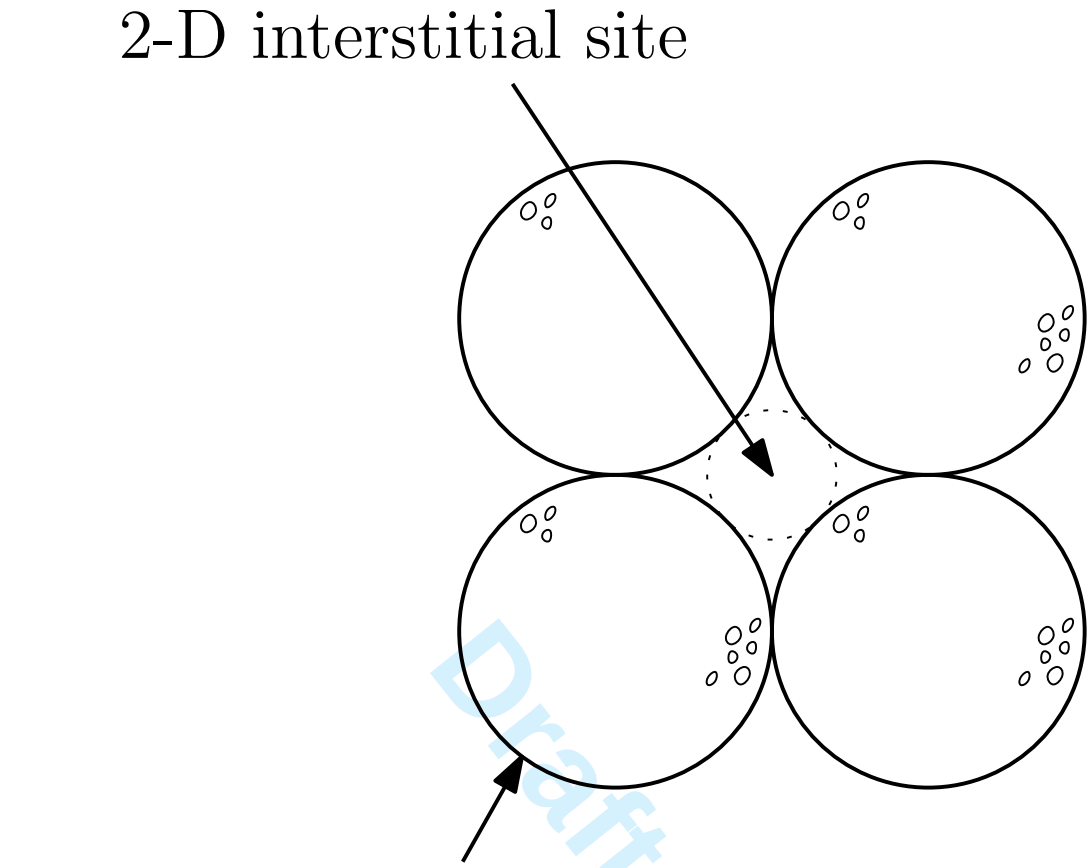

Fig. 3. Interstitial pore space between cubically-packed spherical particles

Draft

©xxxx NRC Canada

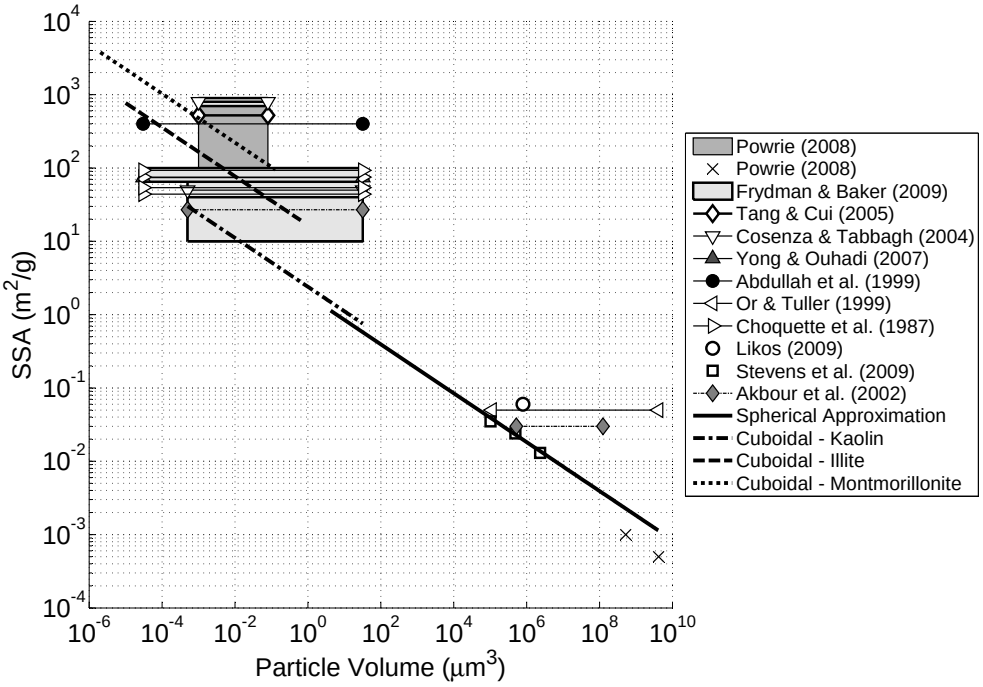

Fig. 4. Specific surface area data (sources given in the figure) compared to spherical and cuboid particle shape approximations

©xxxx NRC Canada

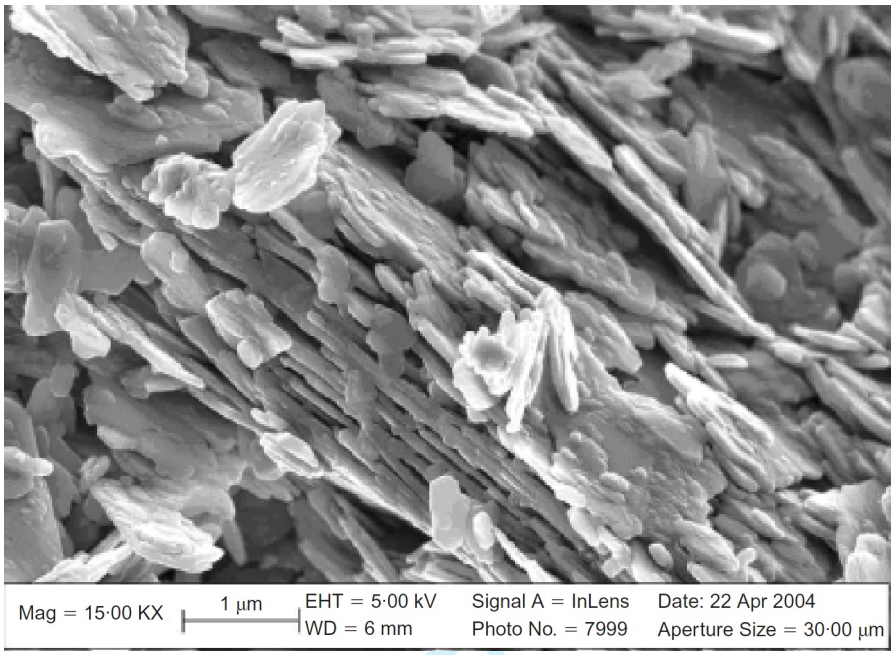

Draft

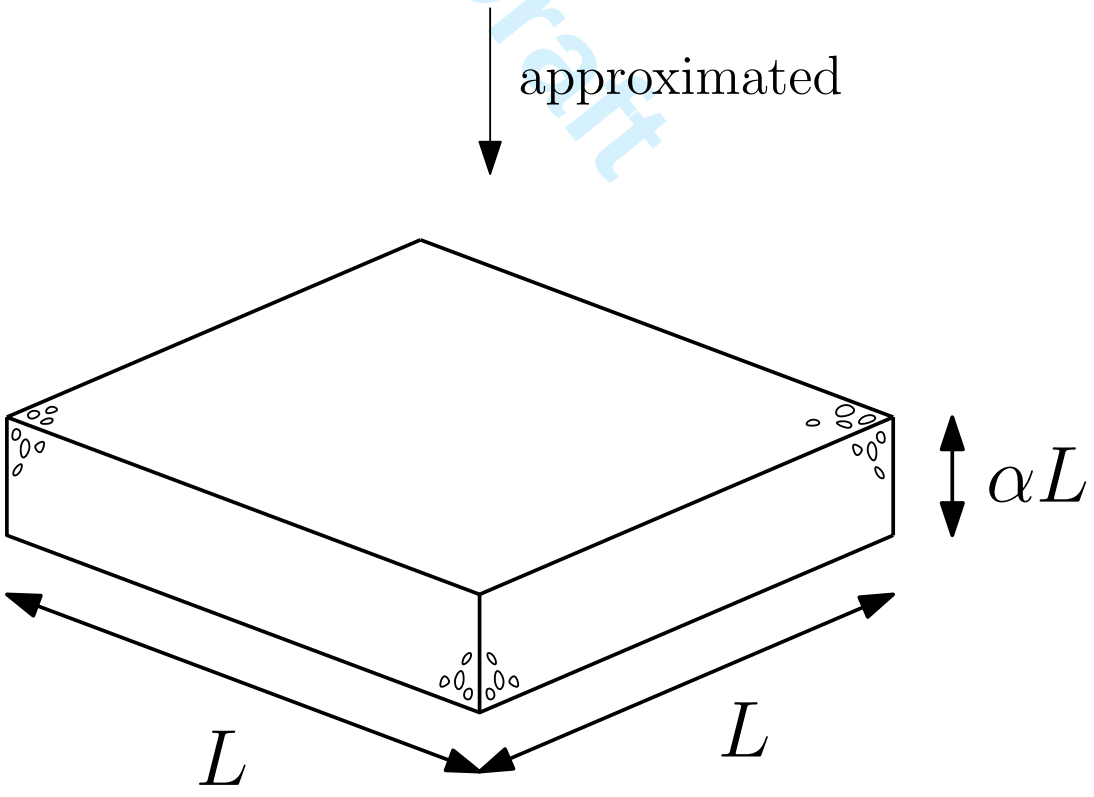

Fig. 5. Cuboidal shape assumption for plate-like particles

©xxxx NRC Canada

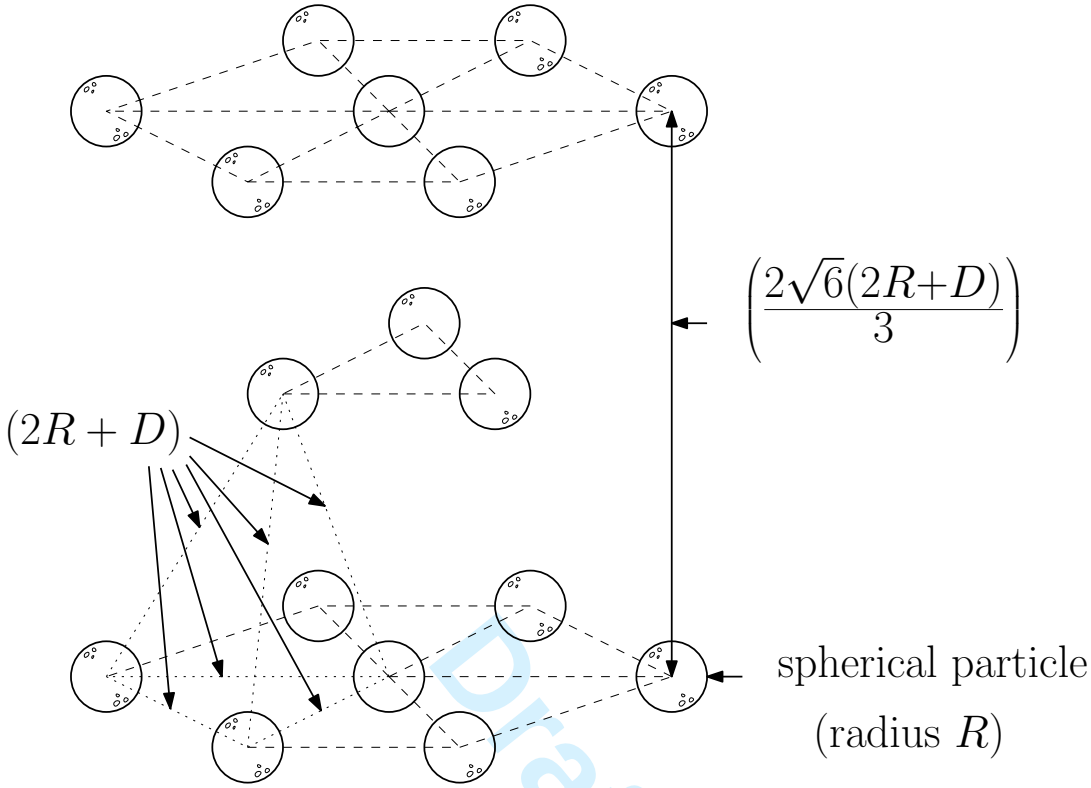

Fig. 6. Enlarged unit cell for tetrahedral sphere packing. Dotted lines show the shape of a single tetrahedral unit cell.

Draft

©xxxx NRC Canada

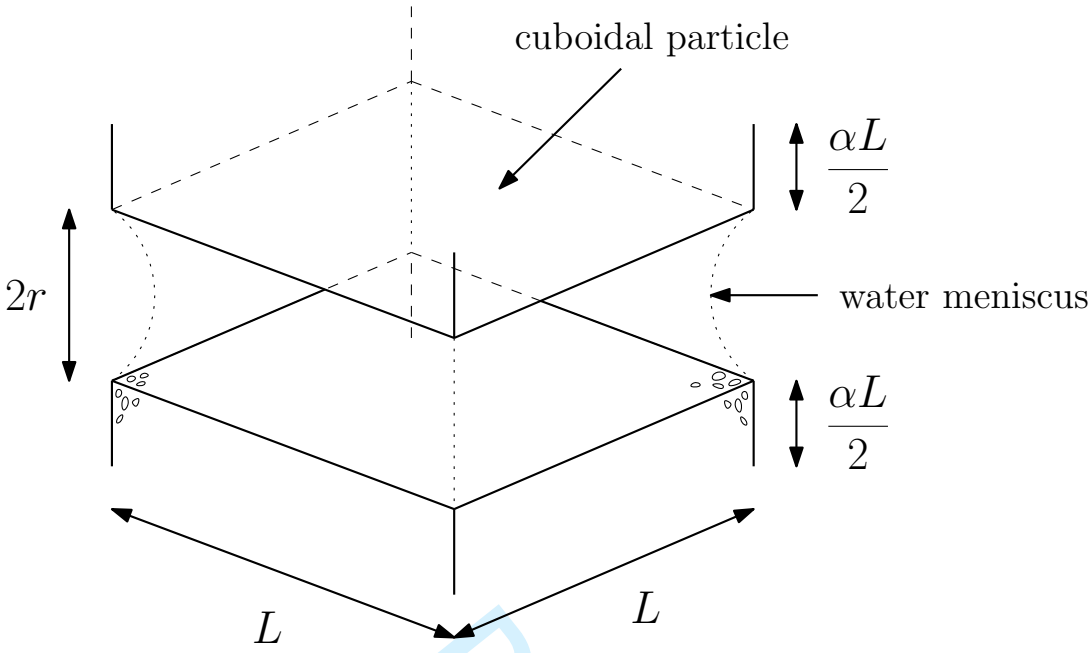

Fig. 7. Cuboidal particle unit cell (assumed example water menisci profiles also shown)

Draft

©xxxx NRC Canada

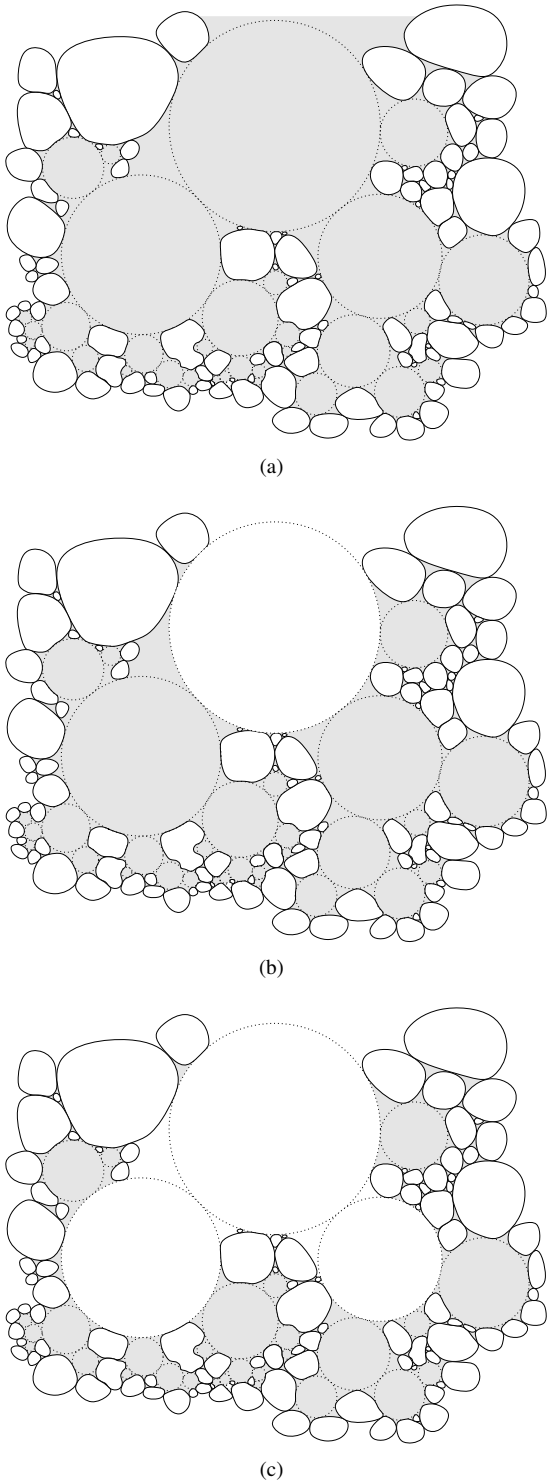

Fig. 8. Desaturation of an example granular soil comprising rounded particles through cavitation of spherical interstitial pores: a) saturated; b) initial desaturation; c) progressive cavitation at higher suctions

©xxxx NRC Canada

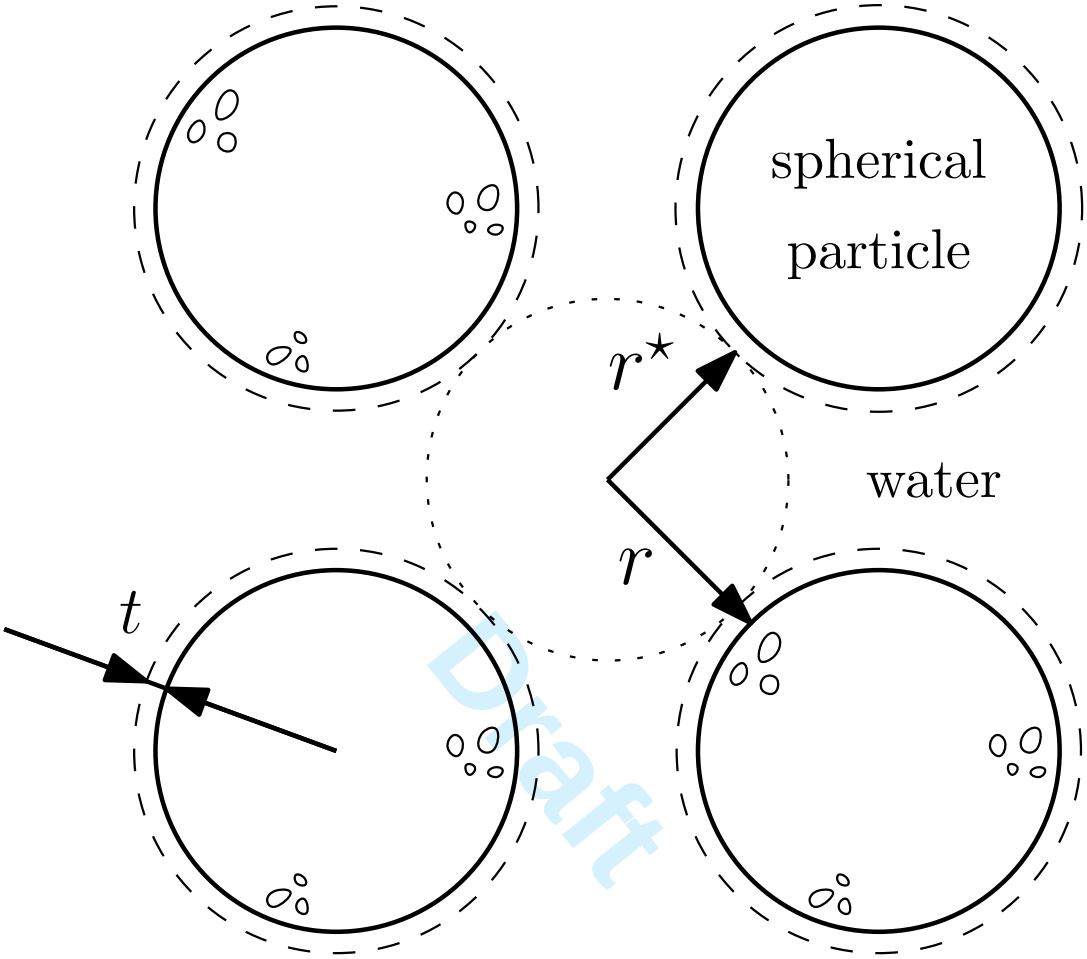

Fig. 9. Reduced cavitation radius due to adsorbed films

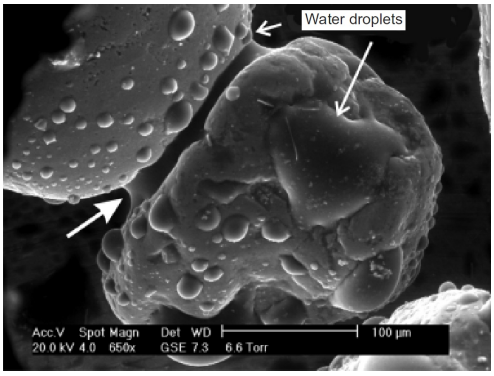

Fig. 10. ESEM micrograph of granular particles undergoing wetting (Lourenço et al., 2012)

©xxxx NRC Canada

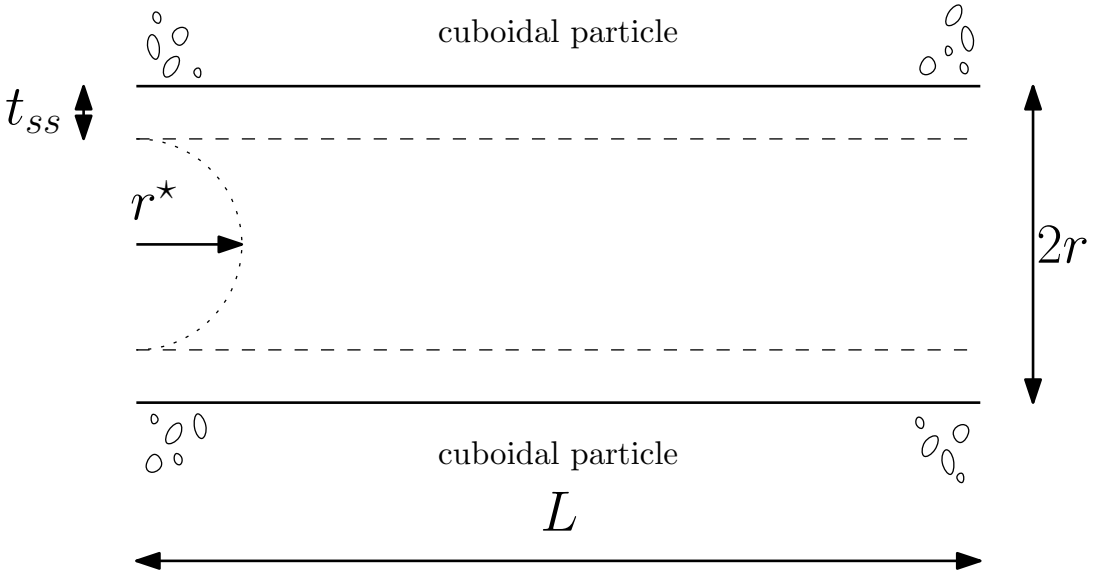

Fig. 11. Cavitation in a slit-shaped pore containing two adsorbed films

Draft

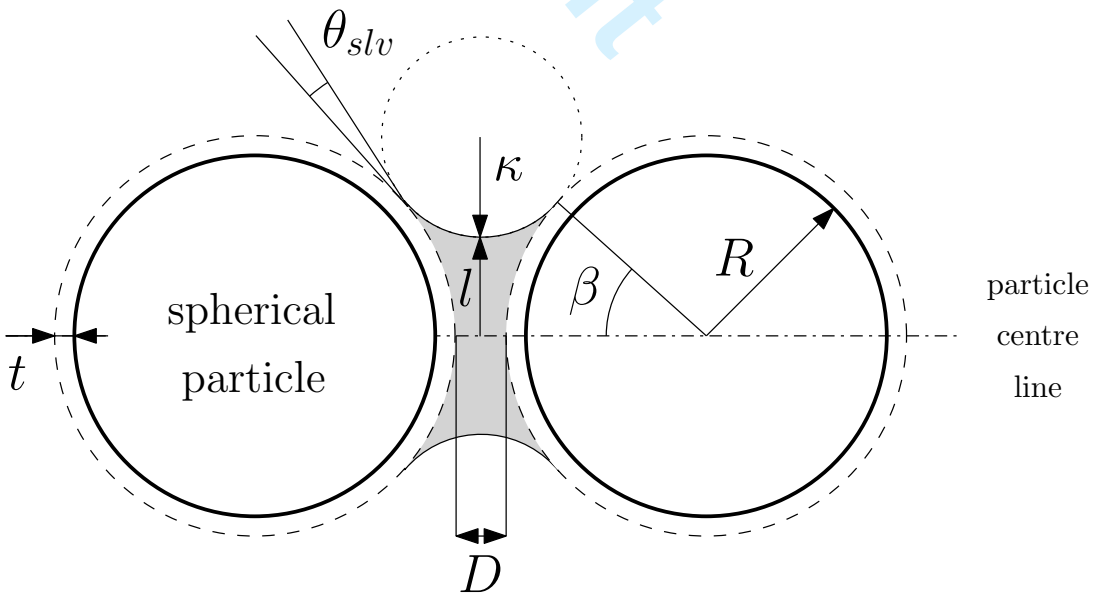

Fig. 12. Liquid bridge parameters

©xxxx NRC Canada

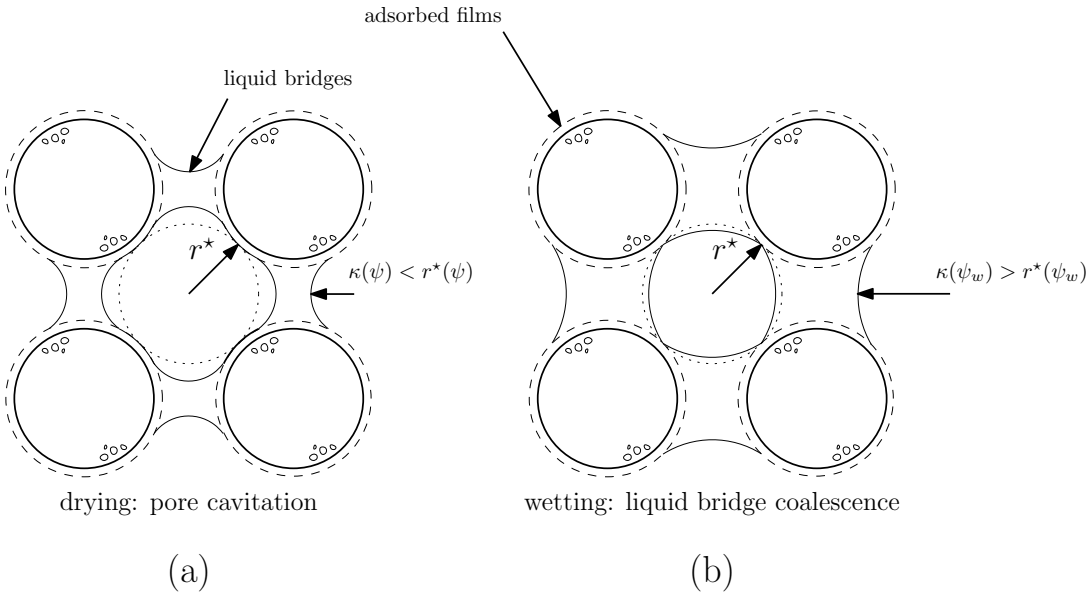

Fig. 13. Drying and wetting liquid bridge configurations

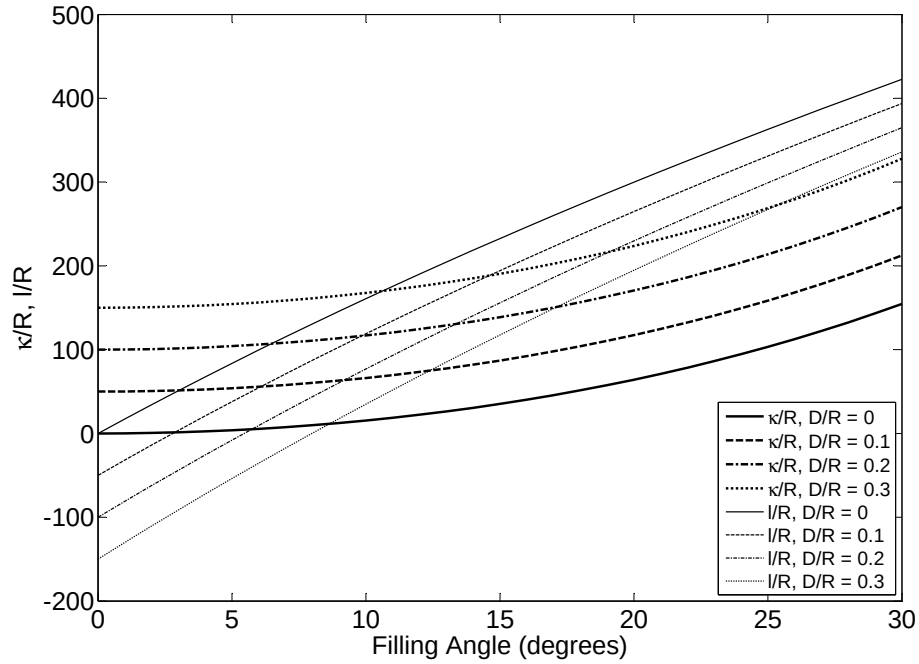

Fig. 14. Effect of separation distance on κ and l, normalised against particle radius R.

©xxxx NRC Canada

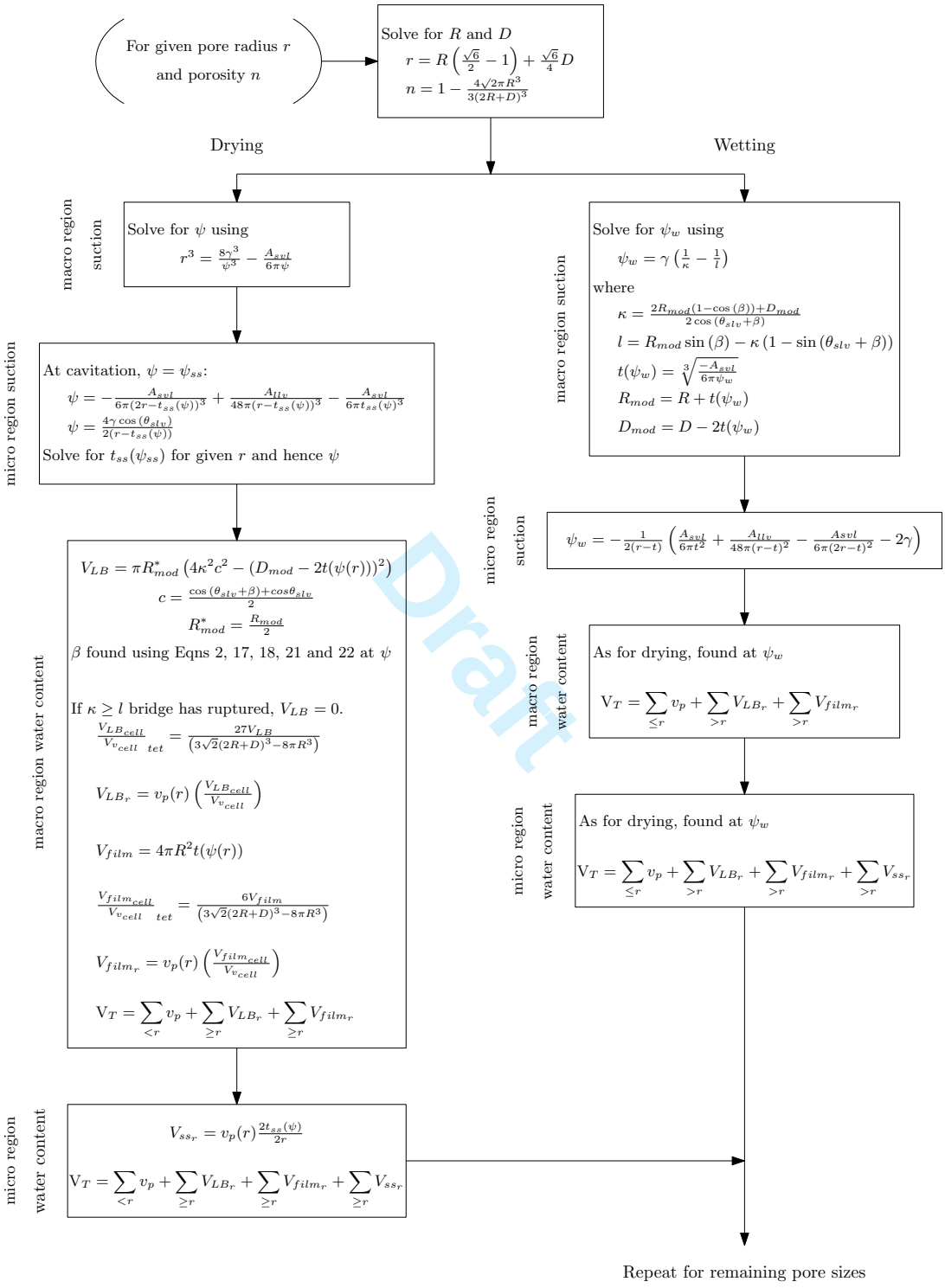

Fig. 15. Summary of equations used to determine the SWRC for a given pore size r and porosity n

©xxxx NRC Canada

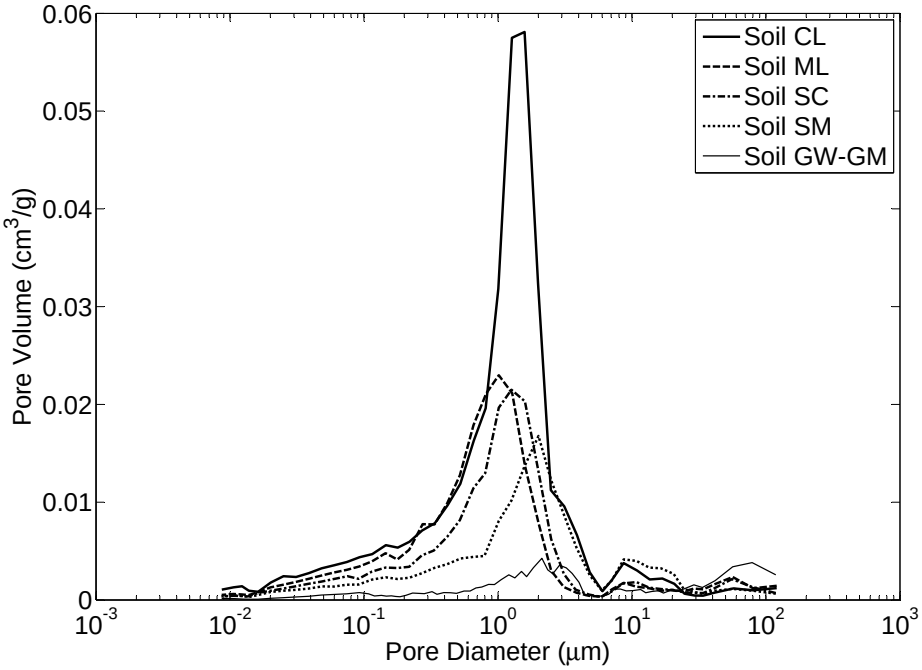

Fig. 16. Pore size distributions for five colluvial soil types post compaction and saturation Zhang and Li (2010)

©xxxx NRC Canada

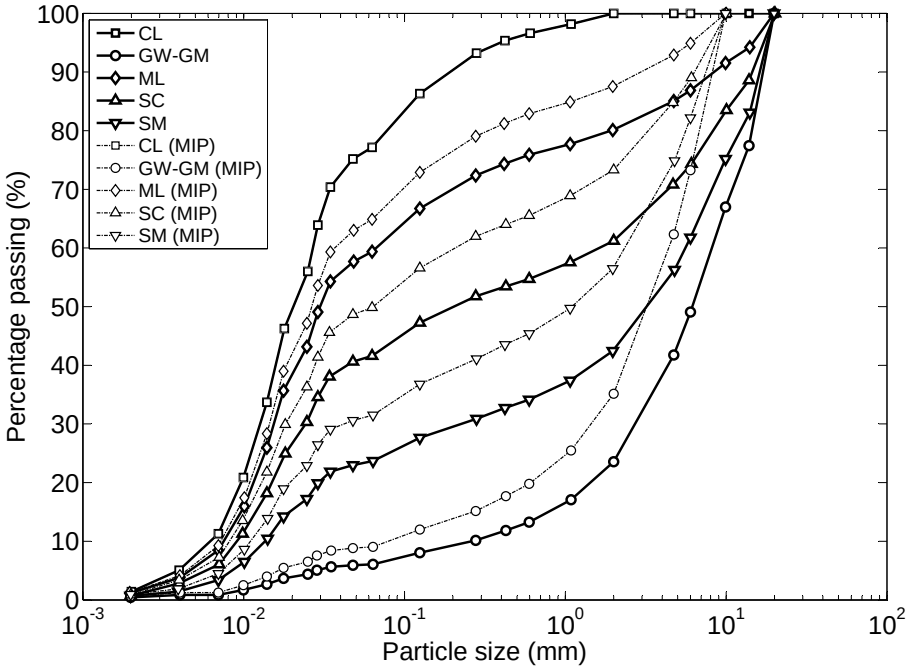

Fig. 17. Particle grading curves for soils tested in Zhang and Li (2010)

©xxxx NRC Canada

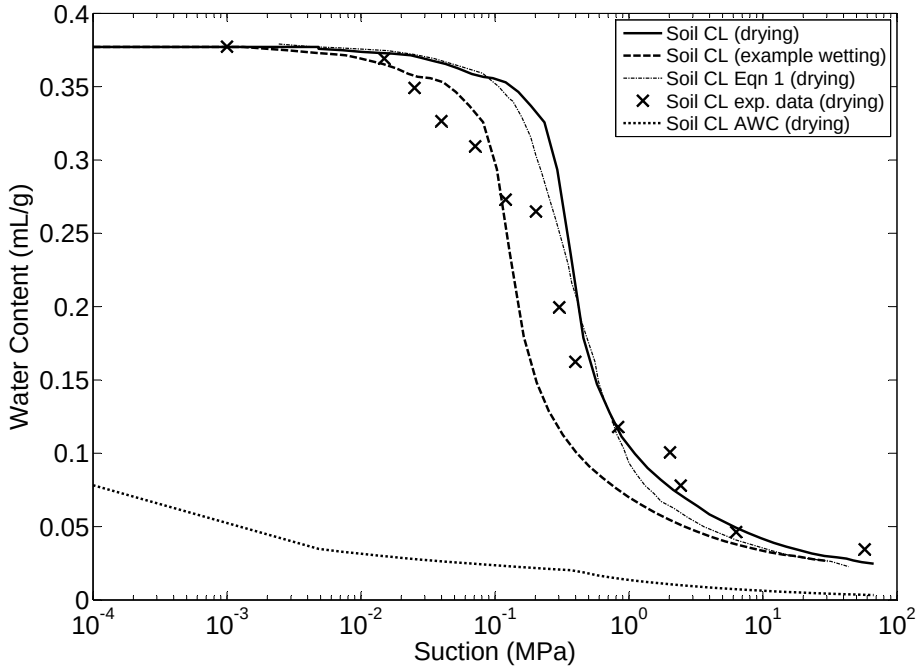

Fig. 18. Predicted SWRCs for soil CL

©xxxx NRC Canada

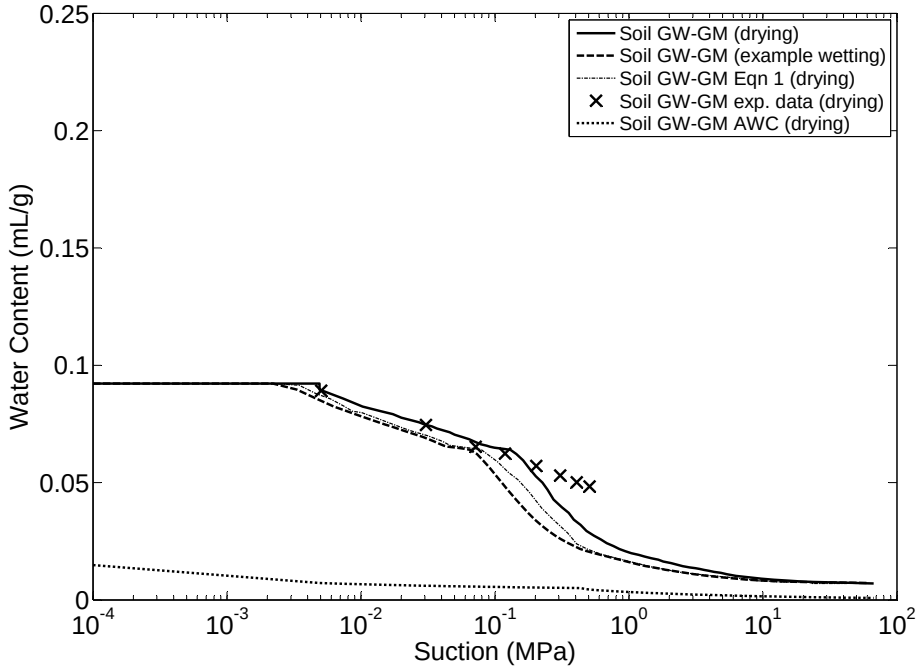

Fig. 19. Predicted SWRCs for soil GWGM

©xxxx NRC Canada

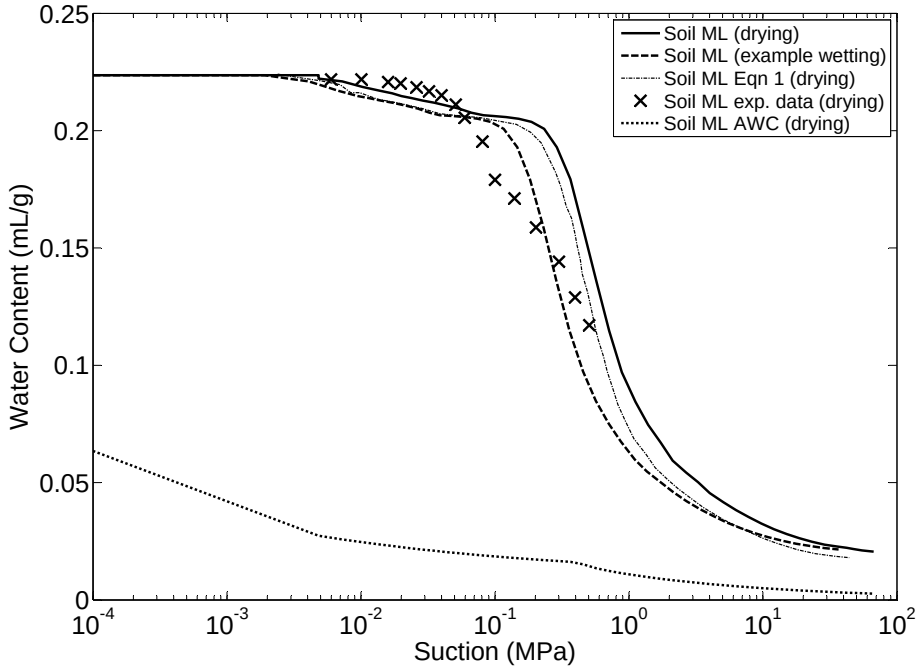

Fig. 20. Predicted SWRCs for soil ML

©xxxx NRC Canada

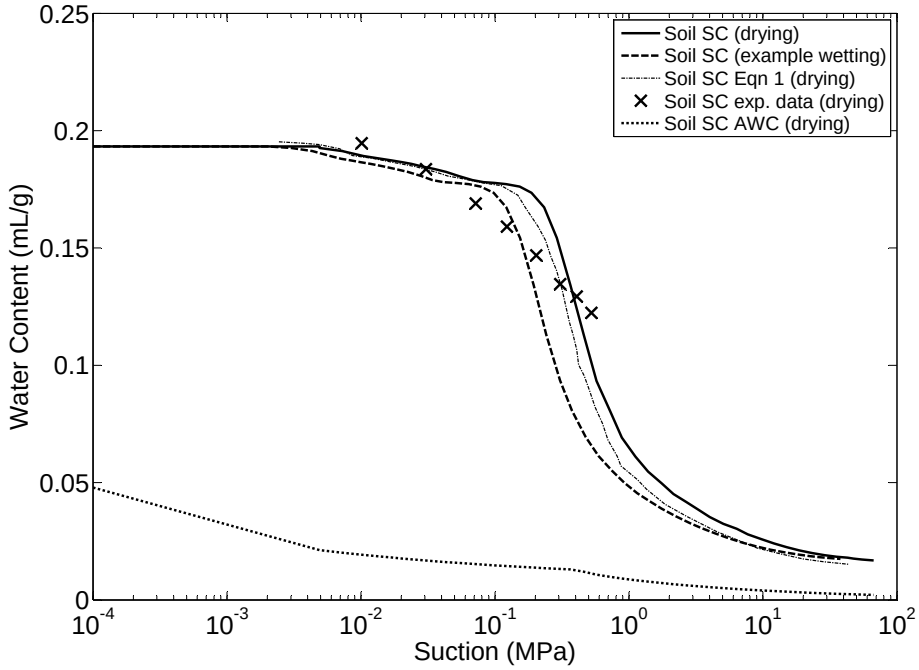

Fig. 21. Predicted SWRCs for soil SC

©xxxx NRC Canada

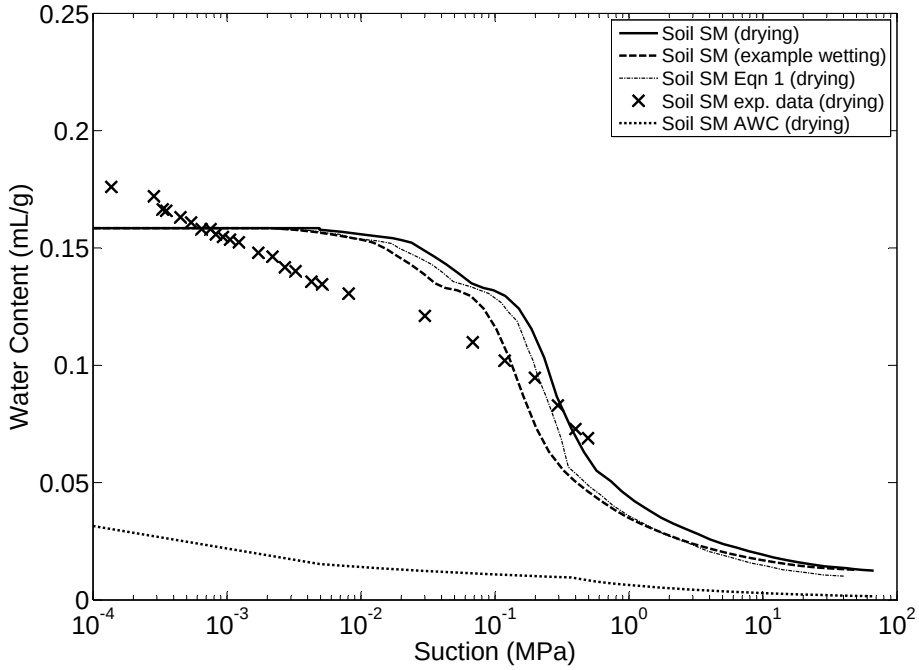

Fig. 22. Predicted SWRCs for soil SM

©xxxx NRC Canada

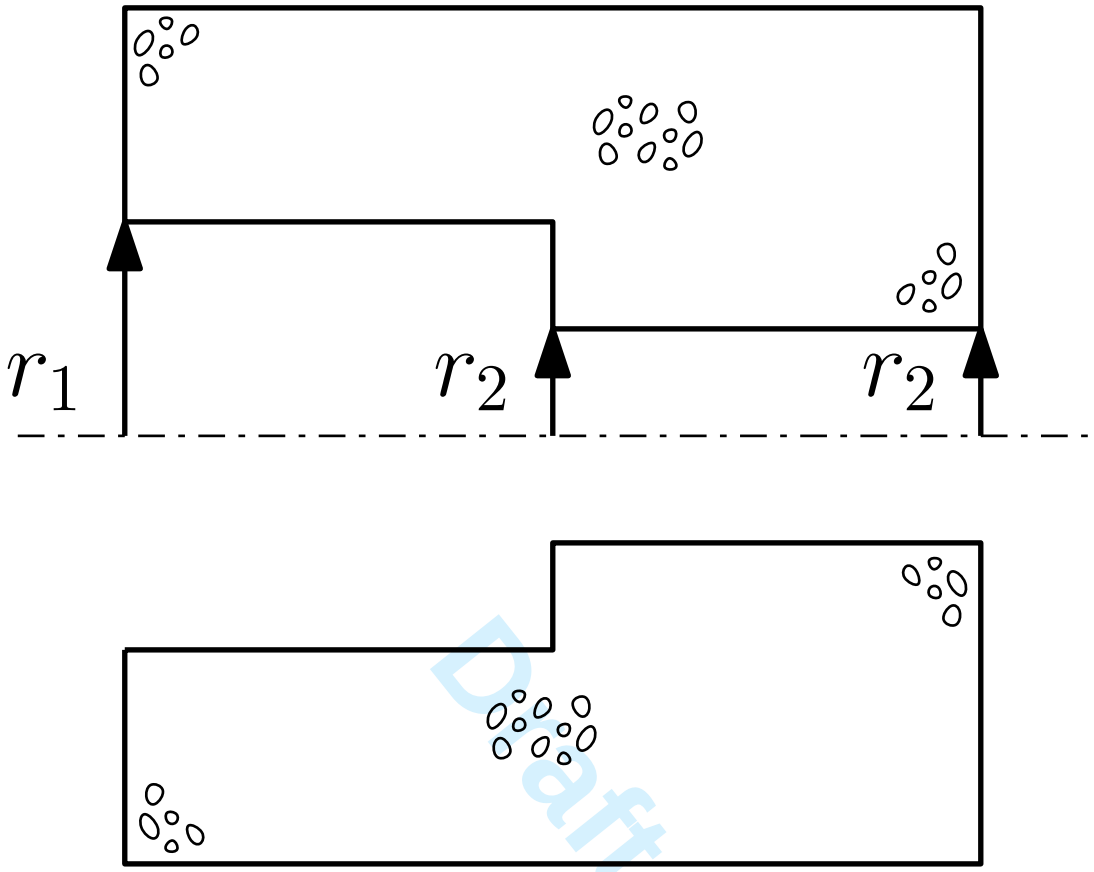

Fig. 23. Changing pore radii in a columnar pore

Draft

©xxxx NRC Canada

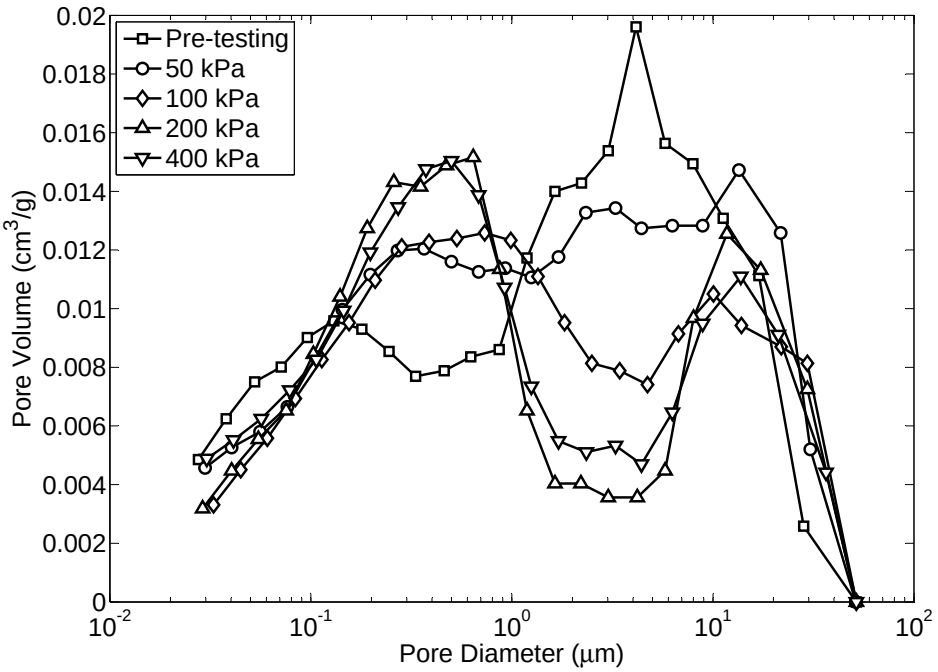

Fig. 24. PSDs for morainic sandy-loam soil after the application of suctions of 0, 50, 100, 200 and 400 kPa (Koliji et al. (2006) after Cuisinier and Laloui (2004))

©xxxx NRC Canada

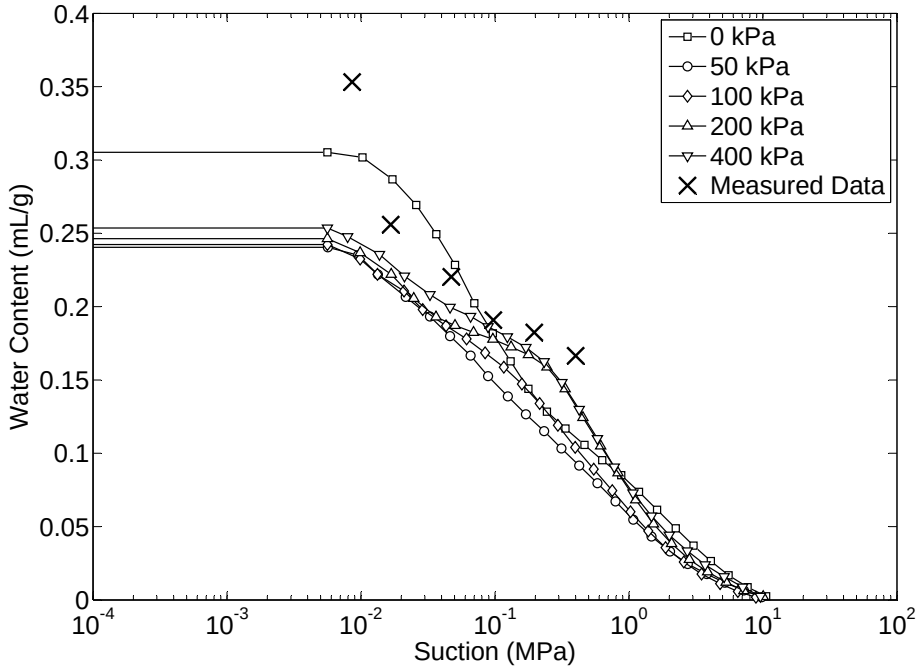

Fig. 25. Predicted SWRCs as compared to measured values (Cuisinier and Laloui, 2004)

©xxxx NRC Canada

Table 1. Particle size values (Powrie, 2008)

Mineral Group	Particle Length (μm)	Particle Thickness (μm)	R (μm)	L (μm)	α
Silt and sand	2 to 2000	2 to 2000	1 to 1000	N/A	N/A
Kaolinite	0.1 to 4	0.05 to 2	N/A	0.1 to 4	0.5
Illite	0.1 to 4	$\geq$0.003	N/A	0.1 to 4	0.01
Montmorillonite	1 to 2	0.001 to 0.02	N/A	0.1 to 4	0.002

Draft

Table 2. Model input (n and θ_{slv}) and output values ($\frac{r}{R}$, $\frac{r}{D}$, r_{lim} and WC$_{lim}$) for predicted drying curves

Soil	n	θ_{slv}	$\frac{r}{R}$	$\frac{r}{D}$	r_{lim} (μm)	WC$_{lim}$ (mL/g)	ψ_{lim} (MPa)
CL	0.50	0	0.40	1.42	0.40	0.0822	1.72
GW-GM	0.30	0	0.25	6.55	0.25	0.0150	2.28
ML	0.37	0	0.29	2.62	0.29	0.0594	2.12
SC	0.35	0	0.28	3.27	0.28	0.0452	2.15
SM	0.32	0	0.26	4.51	0.26	0.0325	2.15

©xxxx NRC Canada

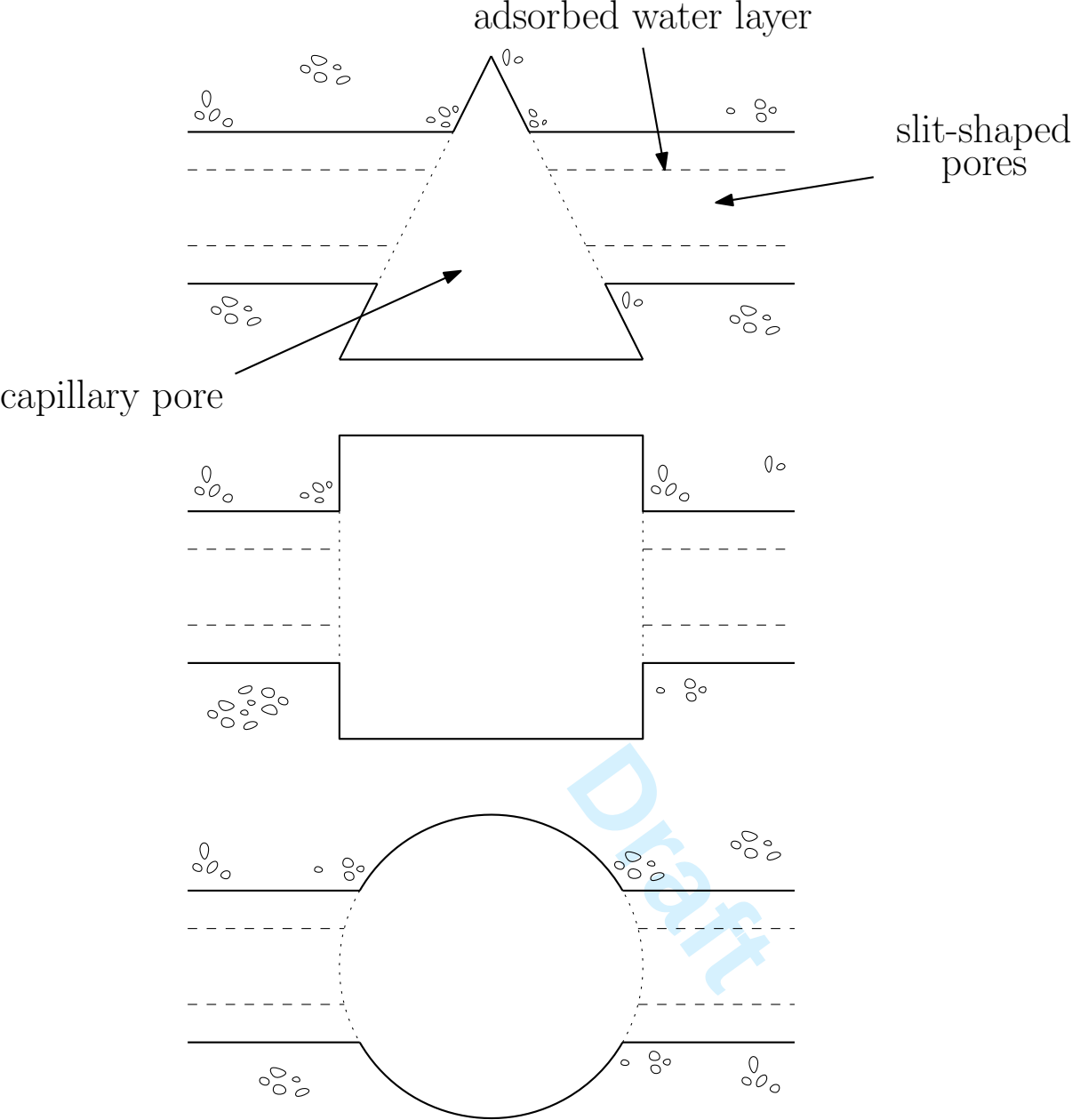

Draft

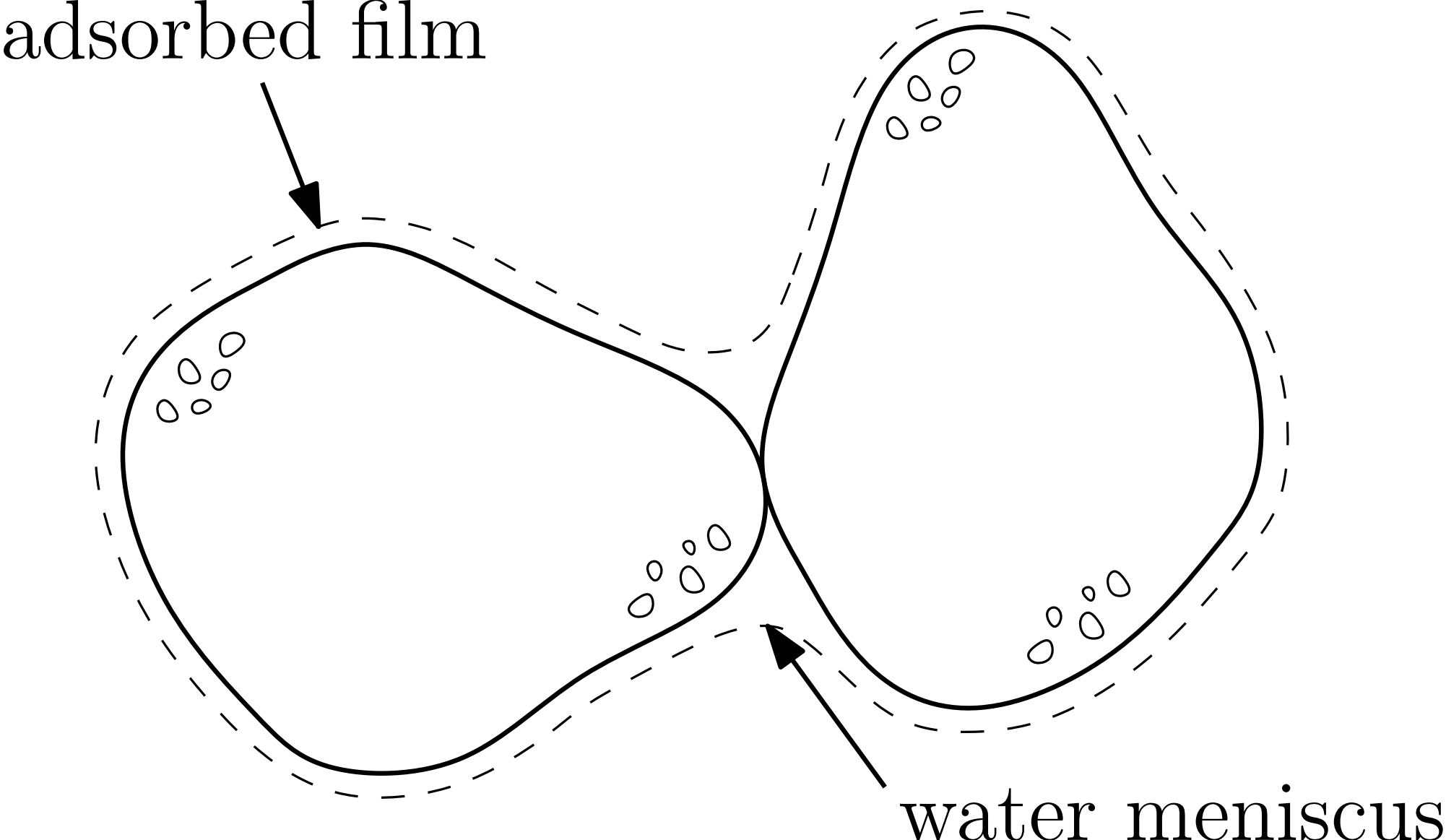
adsorbed film
water meniscus

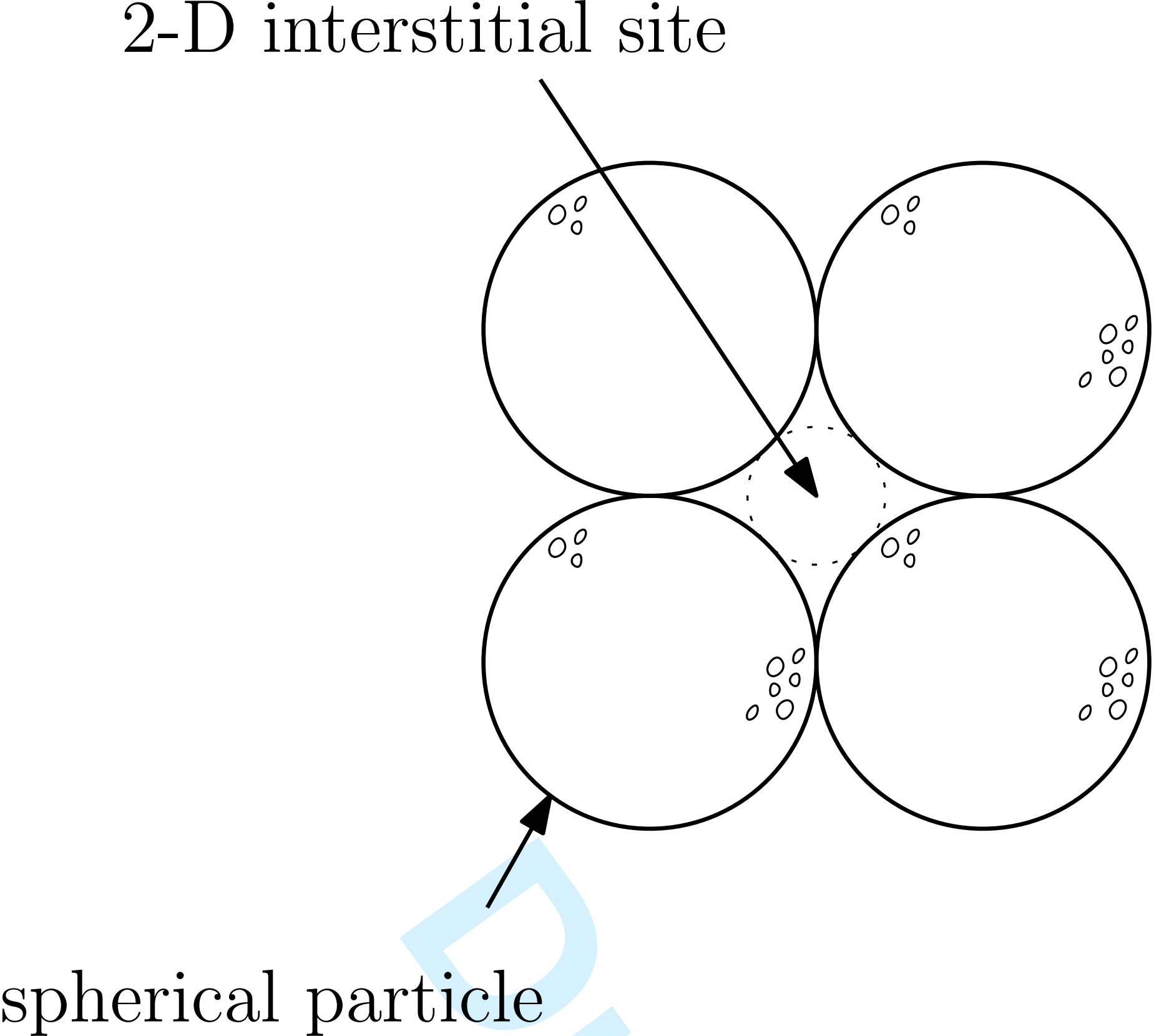
2-D interstitial site
spherical particle

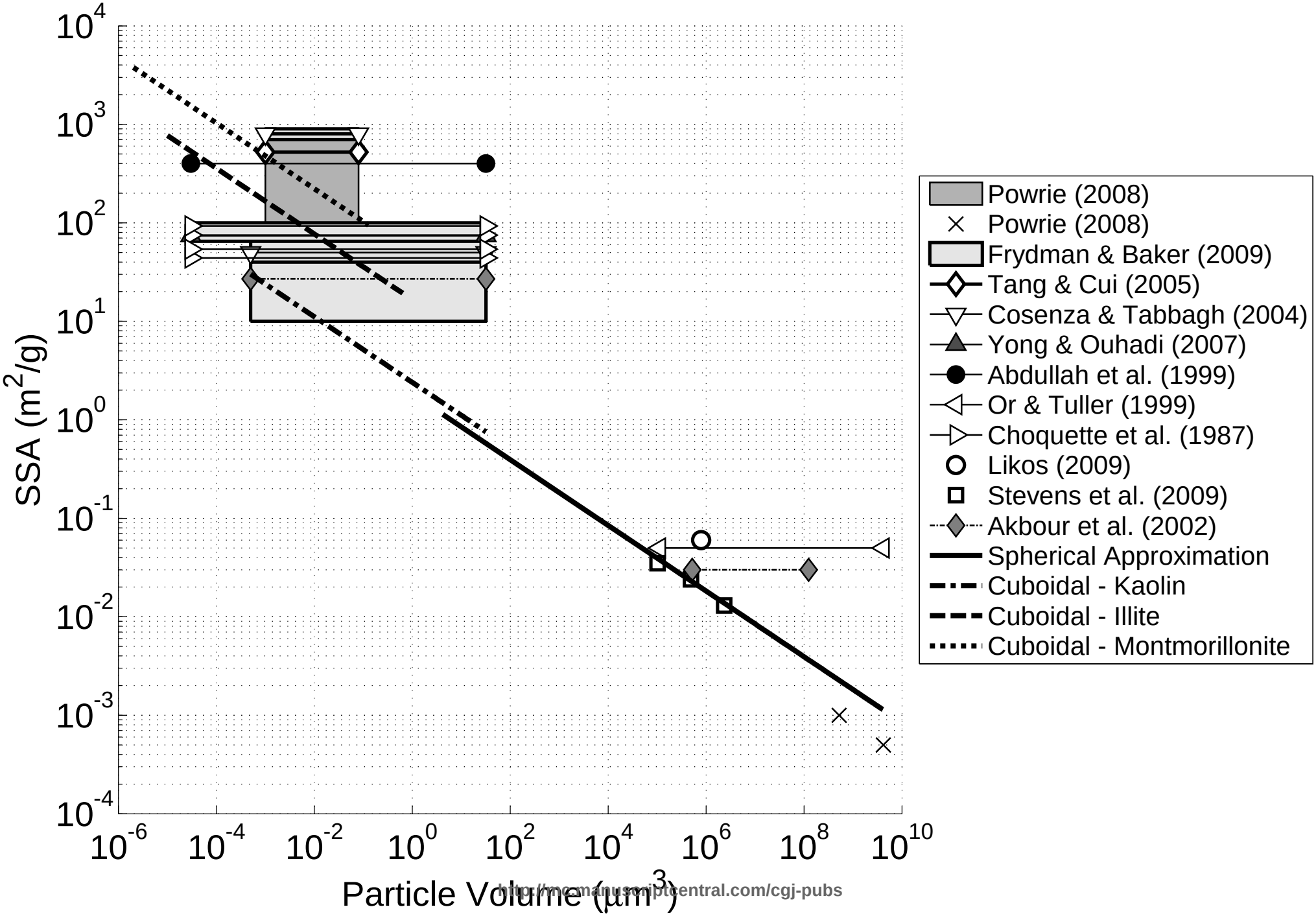
SSA (m2/g)
Particle Volume (μm3)
Powrie (2008)
Powrie (2008)
Frydman & Baker (2009)
Tang & Cui (2005)
Cosenza & Tabbagh (2004)
Yong & Ouhadi (2007)
Abdullah et al. (1999)
Or & Tuller (1999)
Choquette et al. (1987)
Likos (2009)
Stevens et al. (2009)
Akbour et al. (2002)
Spherical Approximation
Cuboidal - Kaolin
Cuboidal - Illite
Cuboidal - Montmorillonite

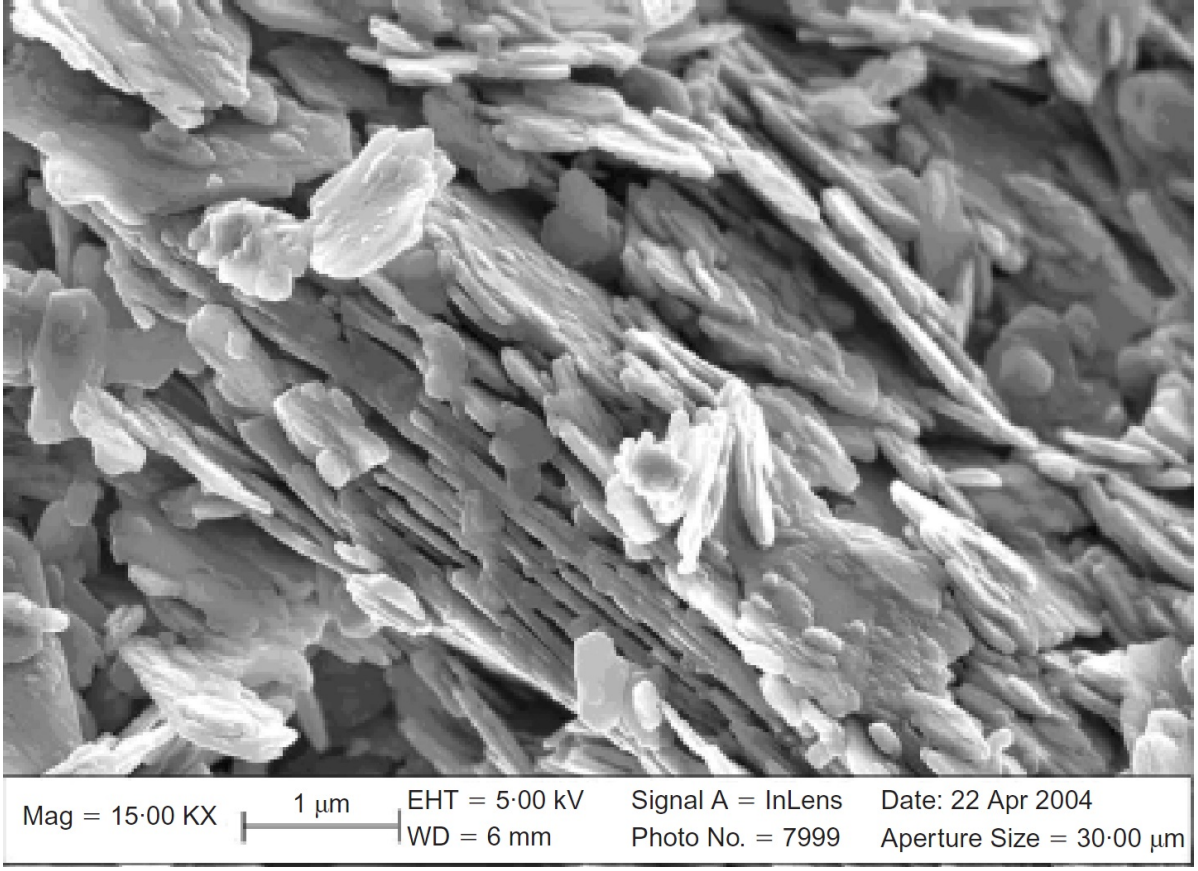

approximated

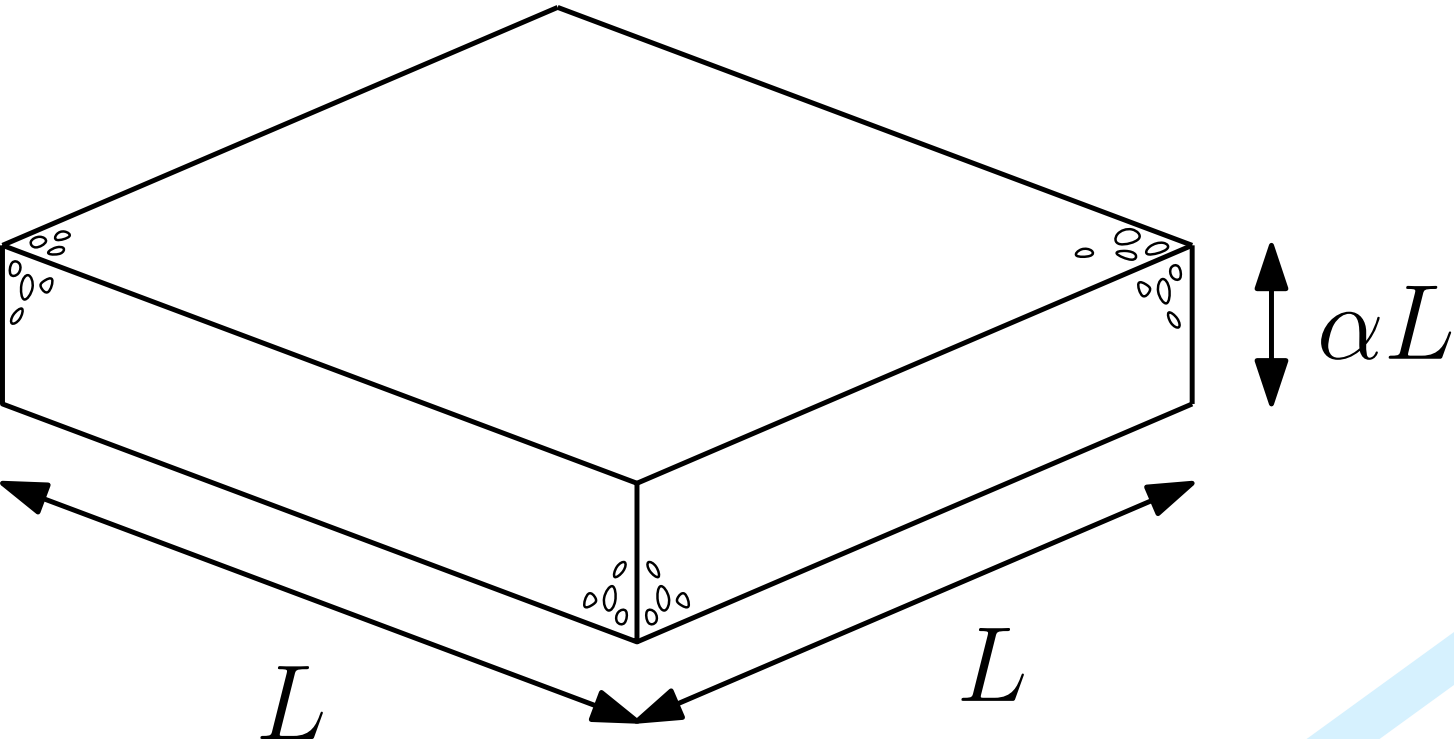

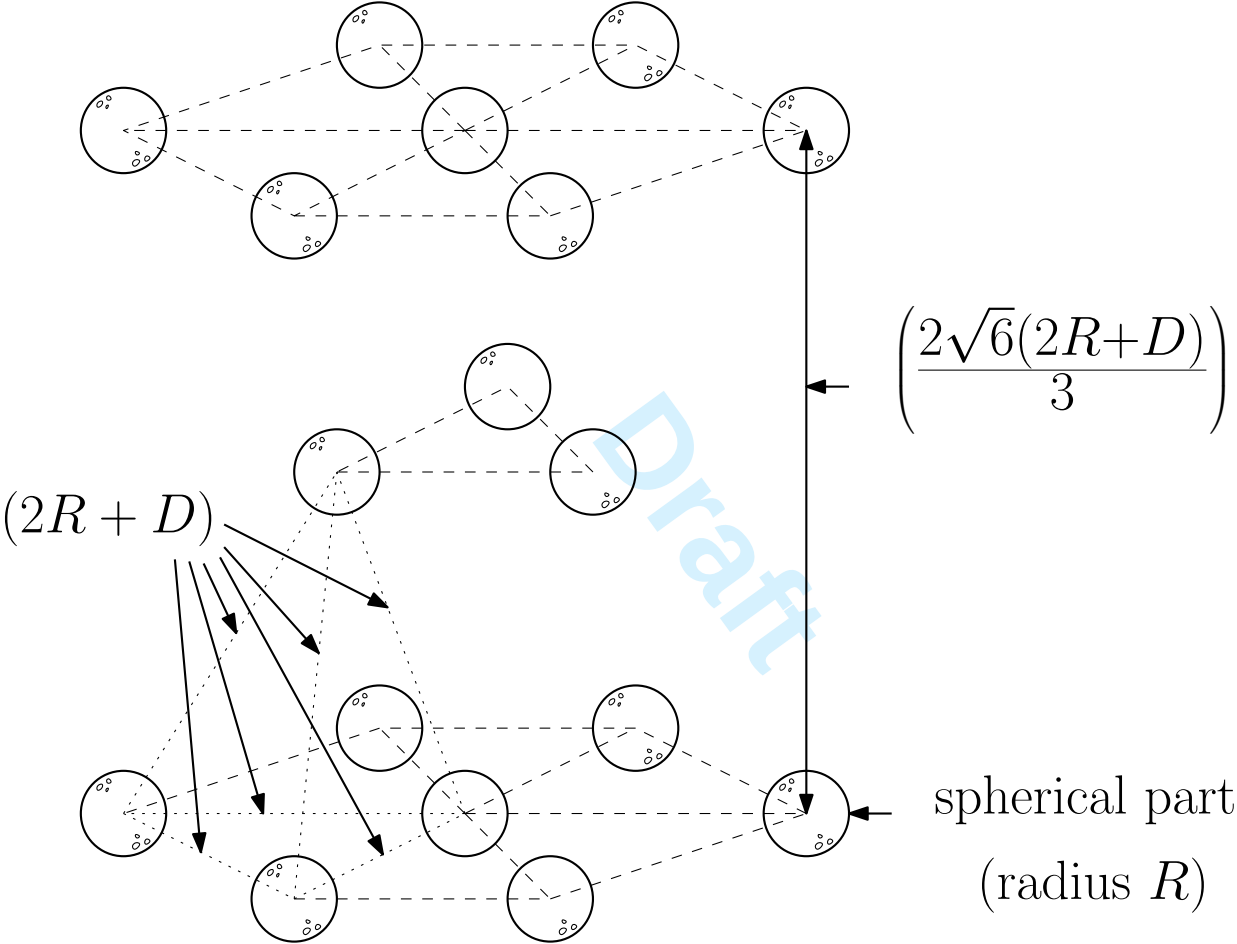
$\left(\frac{2\sqrt{6}(2R+D)}{3}\right)$
$(2R+D)$
spherical particle
(radius R)
Draft

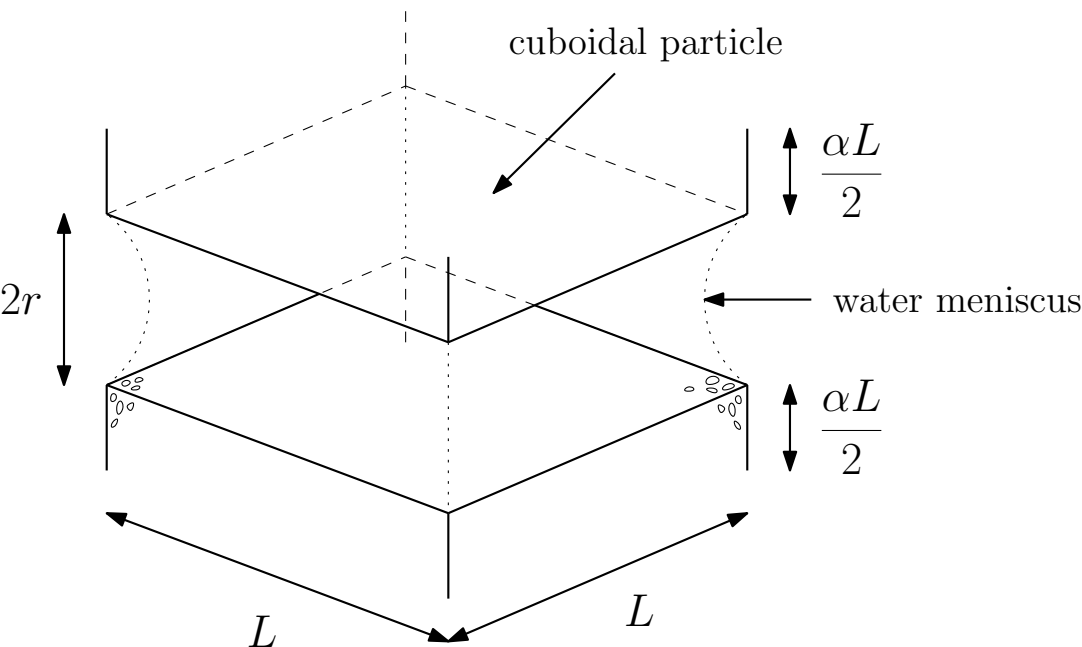
cuboidal particle
$\frac{\alpha L}{2}$
$2r$
water meniscus
$\frac{\alpha L}{2}$
L
L

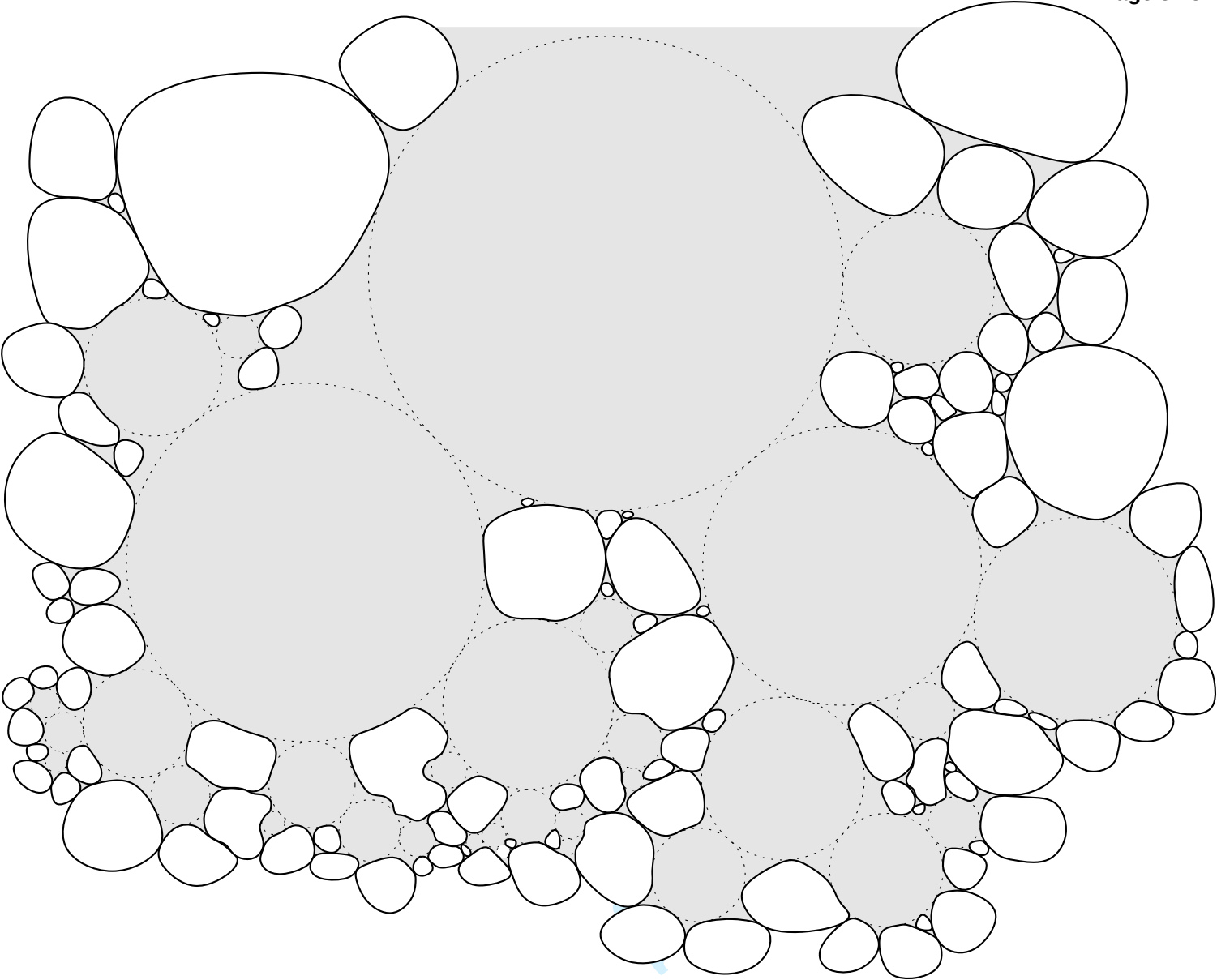

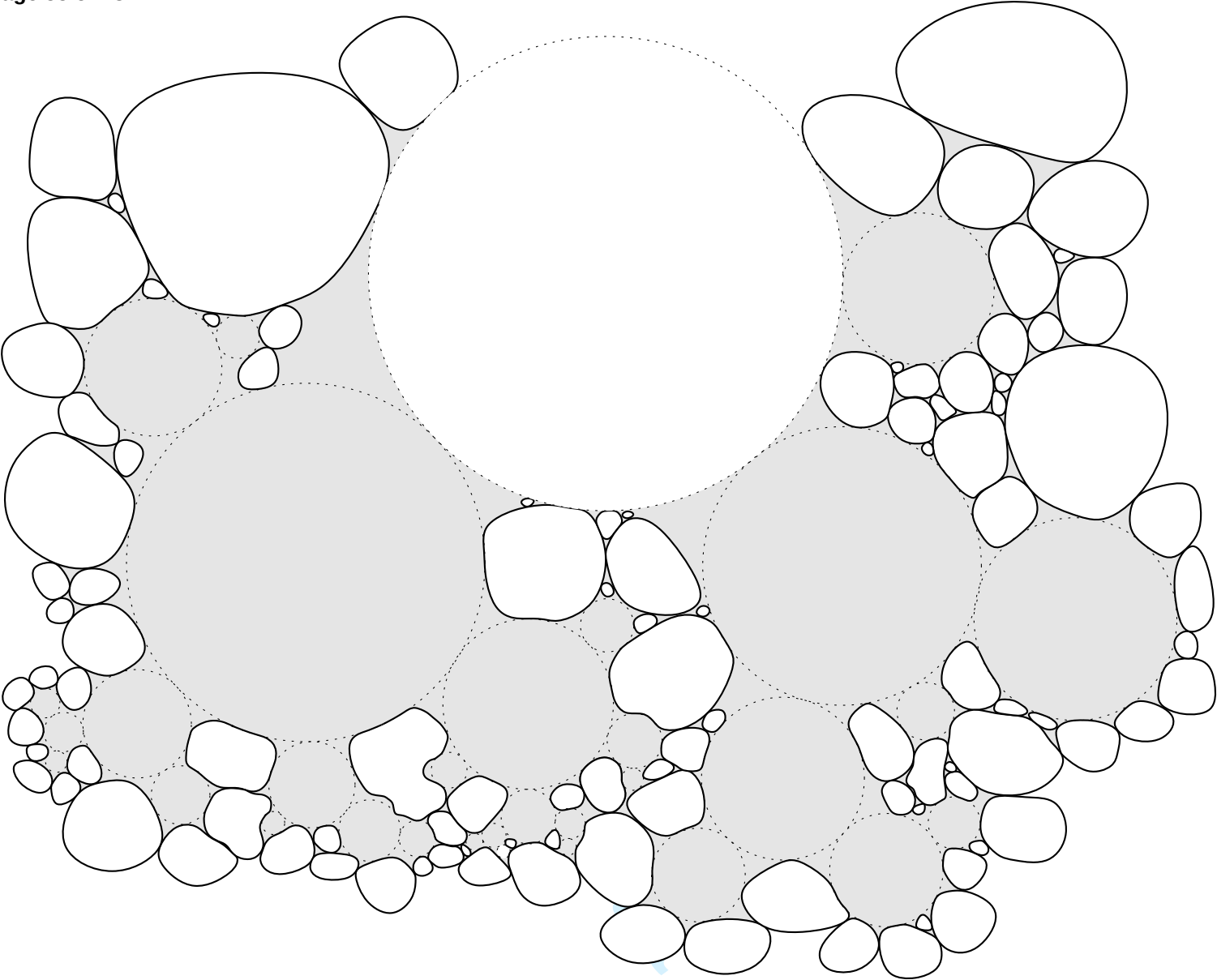

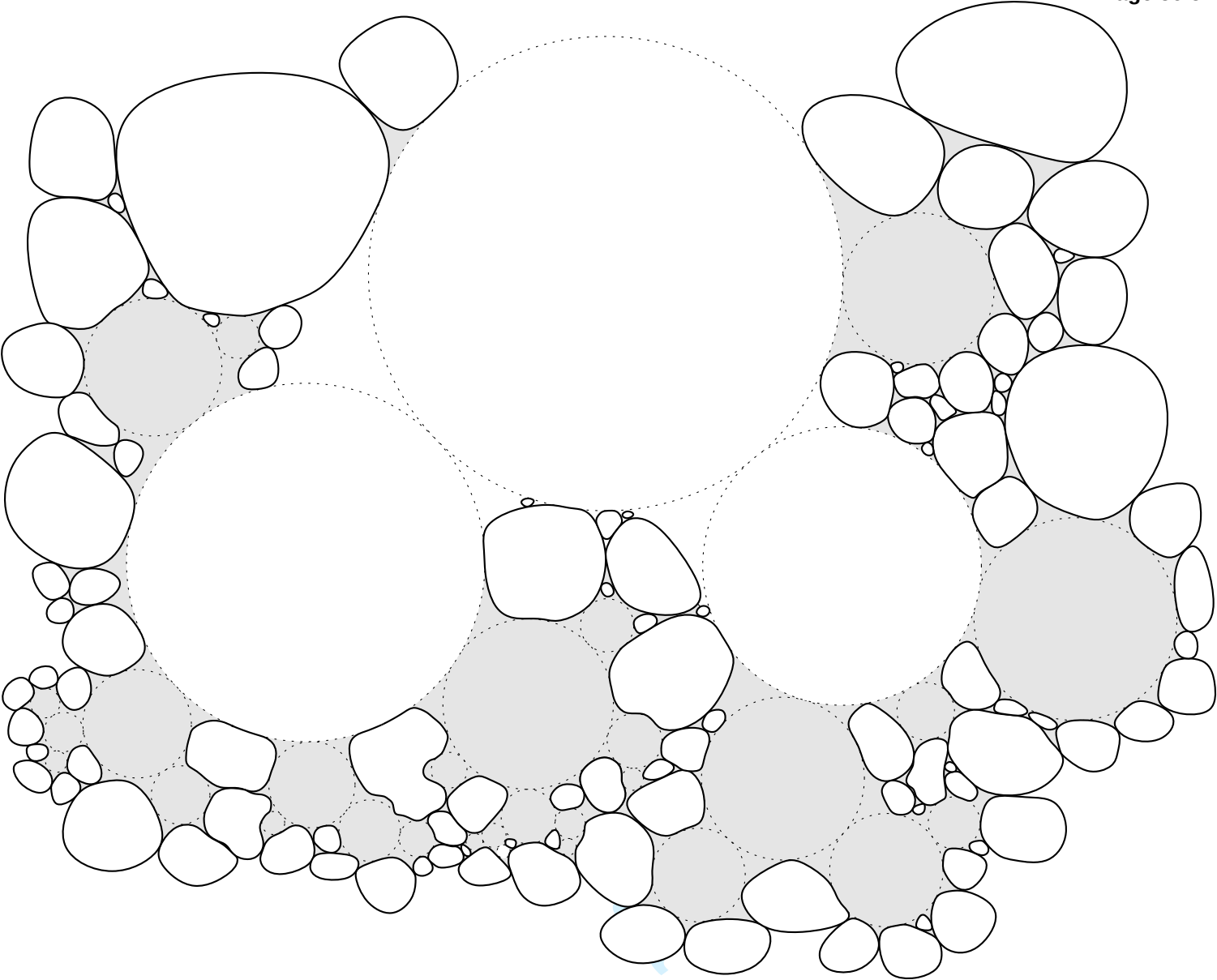

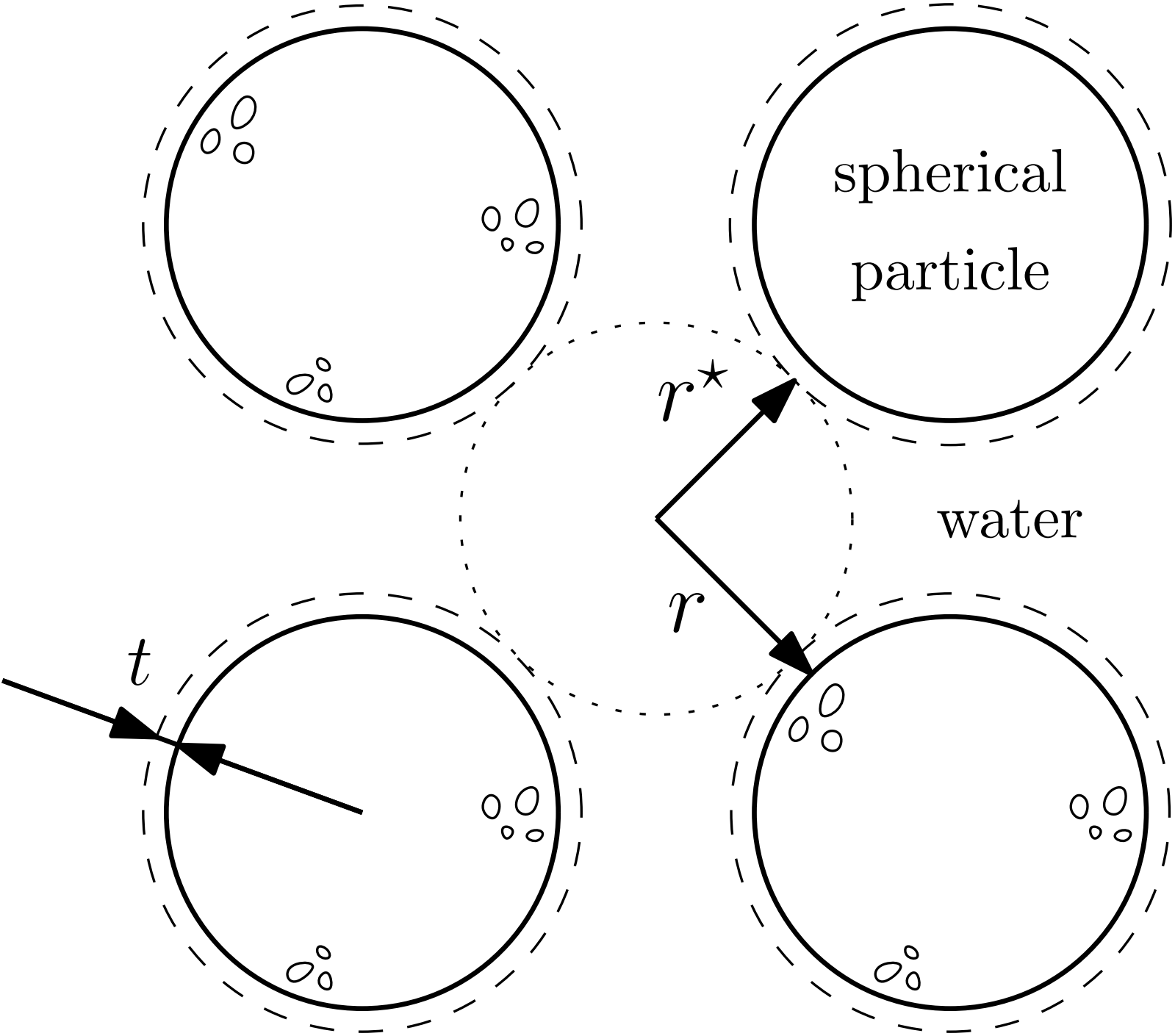
spherical
particle
water
$r^\star$
r
t

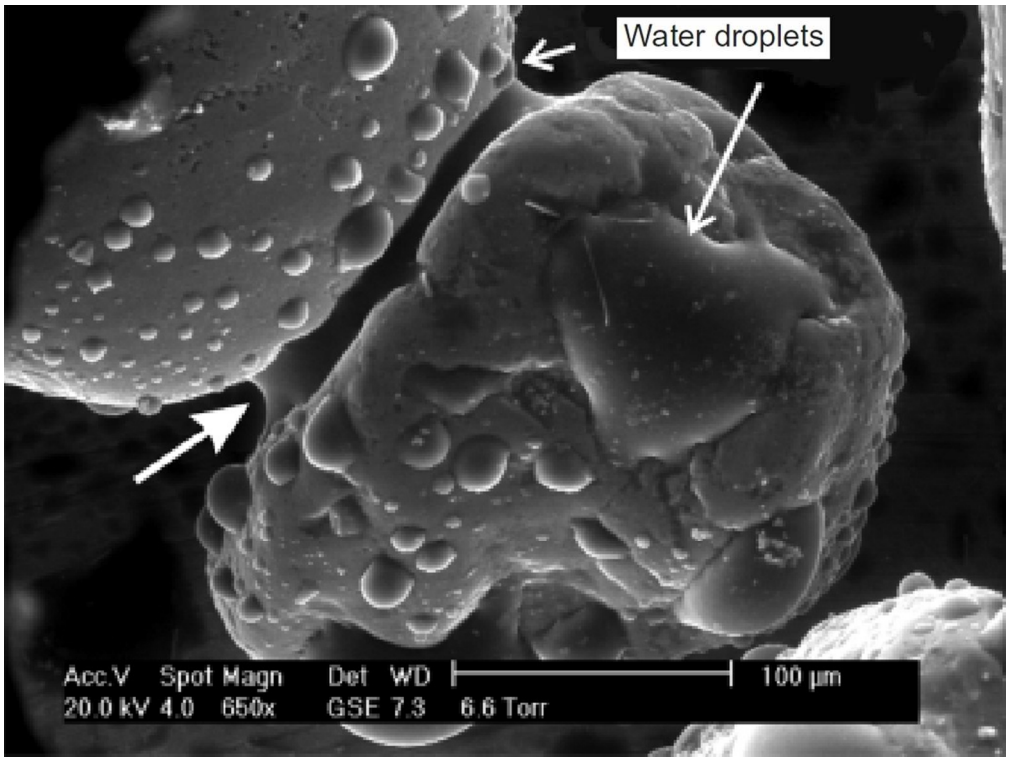

274x206mm (96 x 96 DPI)

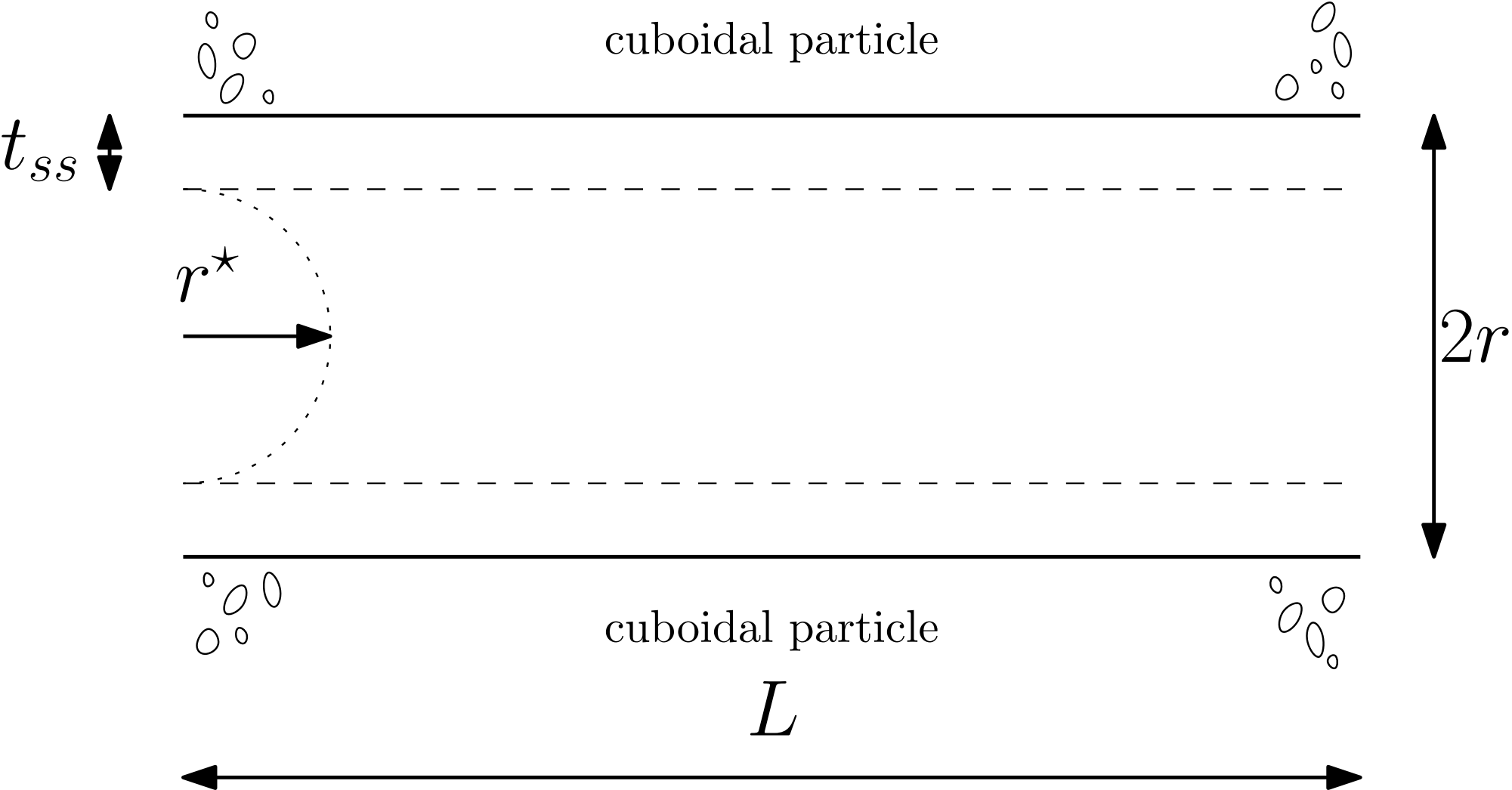
cuboidal particle
t_{ss}
$r^\star$
$2r$
cuboidal particle
L

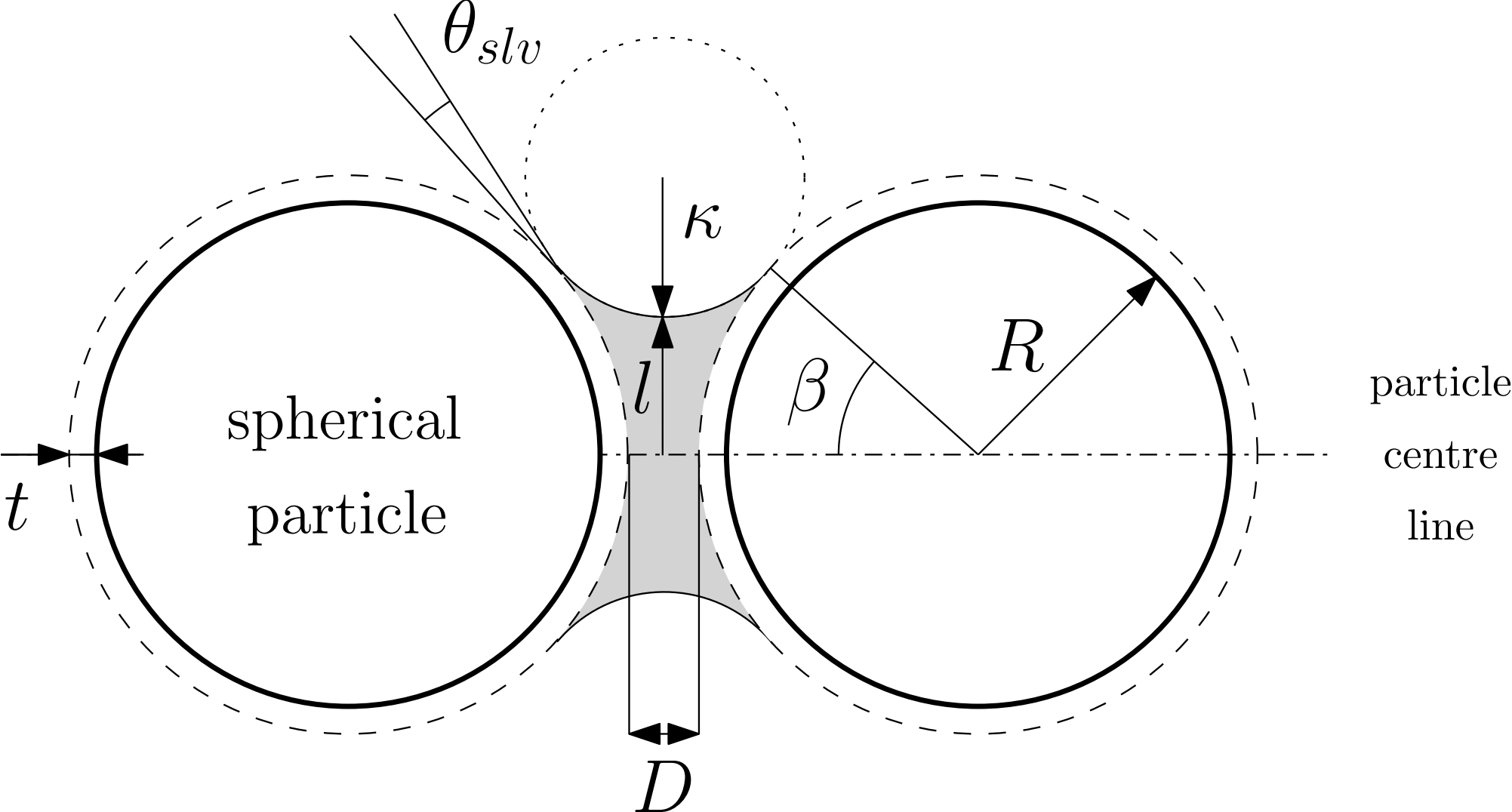
θ_{slv}
κ
l
R
β
spherical
particle
t
D
particle
centre
line

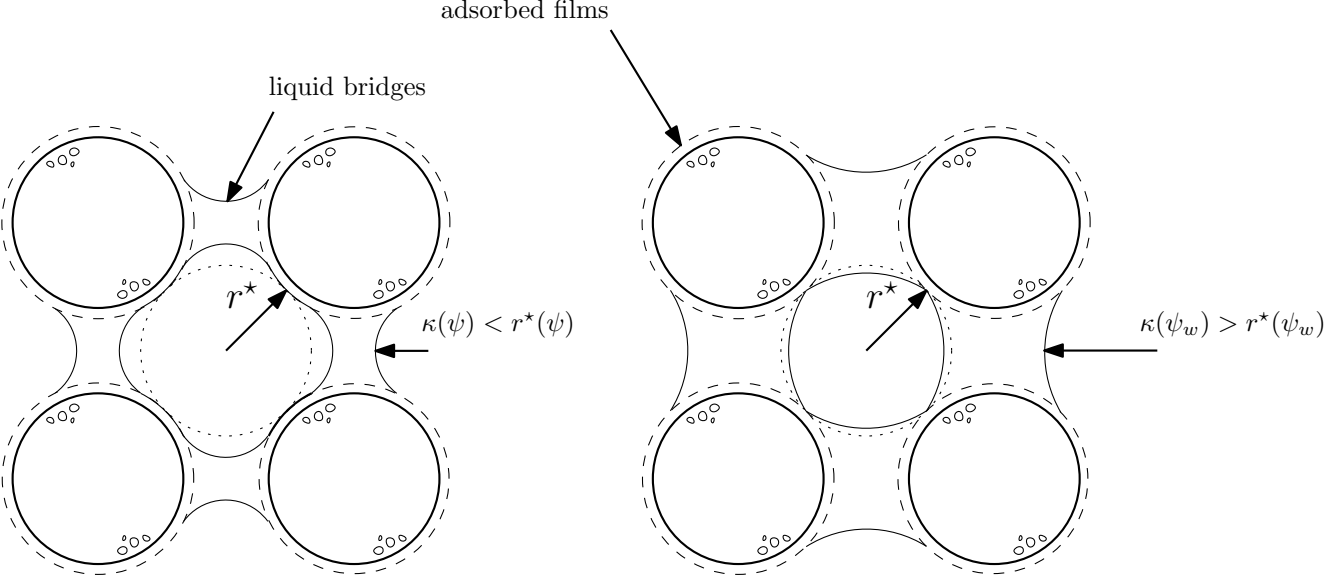
liquid bridges
$r^\star$
$\kappa(\psi) < r^\star(\psi)$
drying: pore cavitation
(a)
adsorbed films
$r^\star$
$\kappa(\psi_w) > r^\star(\psi_w)$
wetting: liquid bridge coalescence
(b)

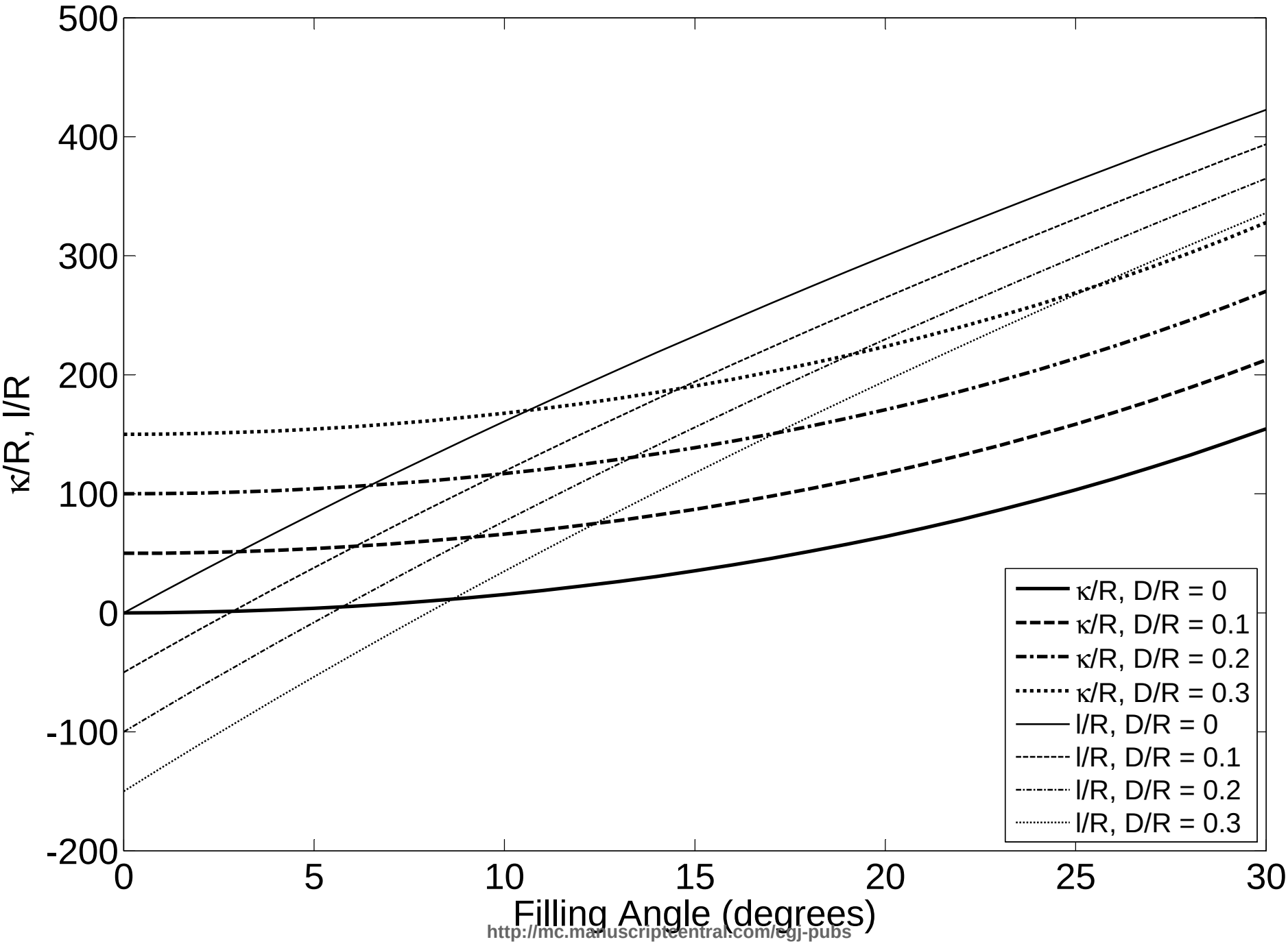
500
400
300
200
100
0
-100
-200
0
5
10
15
20
25
30
κ/R, l/R
Filling Angle (degrees)
κ/R, D/R = 0
κ/R, D/R = 0.1
κ/R, D/R = 0.2
κ/R, D/R = 0.3
l/R, D/R = 0
l/R, D/R = 0.1
l/R, D/R = 0.2
l/R, D/R = 0.3

For given pore radius r and porosity n

Solve for R and D

$$r = R\left(\frac{\sqrt{6}}{2} - 1\right) + \frac{\sqrt{6}}{4}D$$

$$n = 1 - \frac{4\sqrt{2}\pi R^3}{3(2R+D)^3}$$

Drying

Wetting

macro region suction

Solve for ψ using

$$r^3 = \frac{8\gamma^3}{\psi^3} - \frac{A_{svl}}{6\pi\psi}$$

micro region suction

At cavitation, $\psi = \psi_{ss}$:

$$\psi = -\frac{A_{svl}}{6\pi(2r - t_{ss}(\psi))^3} + \frac{A_{llv}}{48\pi(r - t_{ss}(\psi))^3} - \frac{A_{svl}}{6\pi t_{ss}(\psi)^3}$$

$$\psi = \frac{4\gamma\cos(\theta_{slv})}{2(r - t_{ss}(\psi))}$$

Solve for $t_{ss}(\psi_{ss})$ for given r and hence ψ

macro region water content

$$V_{LB} = \pi R^*_{mod}\left(4\kappa^2c^2 - (D_{mod} - 2t(\psi(r)))^2\right)$$

$$c = \frac{\cos(\theta_{slv}+\beta)+cos\theta_{slv}}{2}$$

$$R^*_{mod} = \frac{R_{mod}}{2}$$

β found using Eqns 2, 17, 18, 21 and 22 at ψ

If $\kappa \geq l$ bridge has ruptured, $V_{LB} = 0$.

$$\frac{V_{LB_{cell}}}{V_{v_{cell}}}_{tet} = \frac{27V_{LB}}{\left(3\sqrt{2}(2R+D)^3 - 8\pi R^3\right)}$$

$$V_{LB_r} = v_p(r)\left(\frac{V_{LB_{cell}}}{V_{v_{cell}}}\right)$$

$$V_{film} = 4\pi R^2 t(\psi(r))$$

$$\frac{V_{film_{cell}}}{V_{v_{cell}}}_{tet} = \frac{6V_{film}}{\left(3\sqrt{2}(2R+D)^3 - 8\pi R^3\right)}$$

$$V_{film_r} = v_p(r)\left(\frac{V_{film_{cell}}}{V_{v_{cell}}}\right)$$

$$V_T = \sum_{<r} v_p + \sum_{\geq r} V_{LB_r} + \sum_{\geq r} V_{film_r}$$

micro region water content

$$V_{ss_r} = v_p(r)\frac{2t_{ss}(\psi)}{2r}$$

$$V_T = \sum_{<r} v_p + \sum_{\geq r} V_{LB_r} + \sum_{\geq r} V_{film_r} + \sum_{\geq r} V_{ss_r}$$

macro region suction

Solve for ψ_w using

$$\psi_w = \gamma\left(\frac{1}{\kappa} - \frac{1}{l}\right)$$

where

$$\kappa = \frac{2R_{mod}(1-\cos(\beta))+D_{mod}}{2\cos(\theta_{slv}+\beta)}$$

$$l = R_{mod}\sin(\beta) - \kappa(1 - \sin(\theta_{slv}+\beta))$$

$$t(\psi_w) = \sqrt[3]{\frac{-A_{svl}}{6\pi\psi_w}}$$

$$R_{mod} = R + t(\psi_w)$$

$$D_{mod} = D - 2t(\psi_w)$$

micro region suction

$$\psi_w = -\frac{1}{2(r-t)}\left(\frac{A_{svl}}{6\pi t^2} + \frac{A_{llv}}{48\pi(r-t)^2} - \frac{Asvl}{6\pi(2r-t)^2} - 2\gamma\right)$$

macro region water content

As for drying, found at ψ_w

$$V_T = \sum_{\leq r} v_p + \sum_{>r} V_{LB_r} + \sum_{>r} V_{film_r}$$

micro region water content

As for drying, found at ψ_w

$$V_T = \sum_{\leq r} v_p + \sum_{>r} V_{LB_r} + \sum_{>r} V_{film_r} + \sum_{>r} V_{ss_r}$$

Repeat for remaining pore sizes

Draft

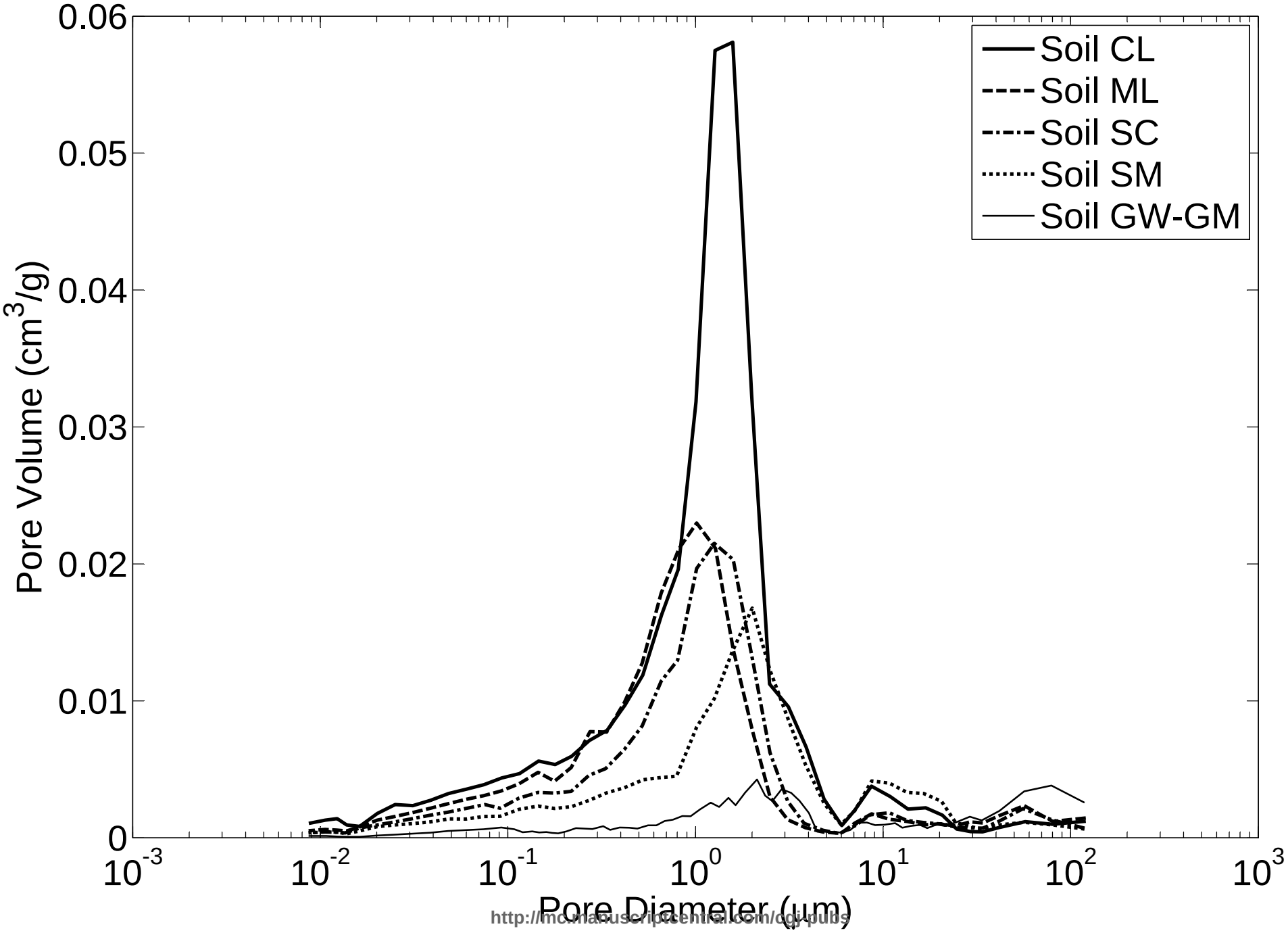

http://mc.manuscriptcentral.com/cgj-pubs

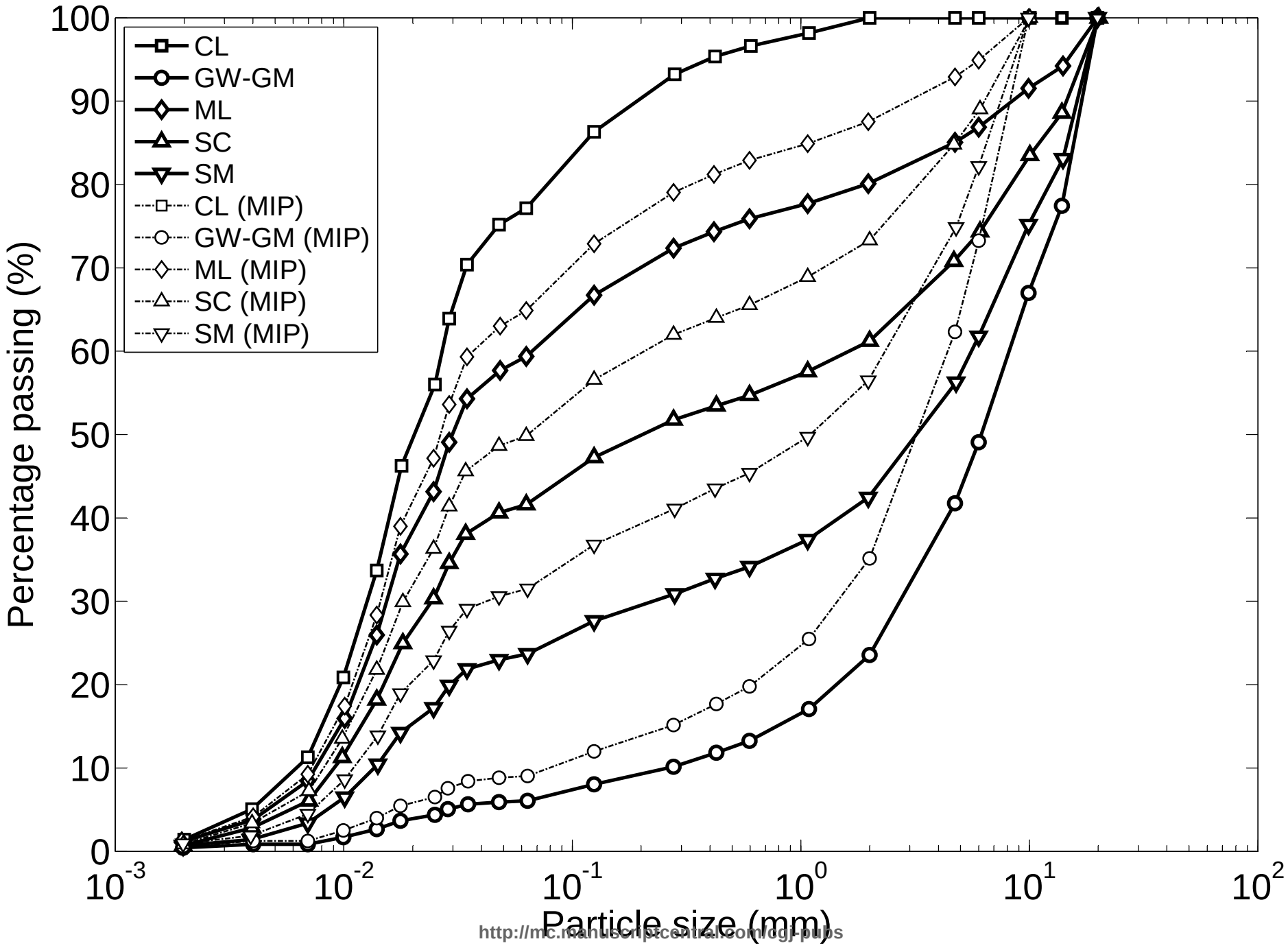

http://mc.manuscriptcentral.com/cgj-pubs

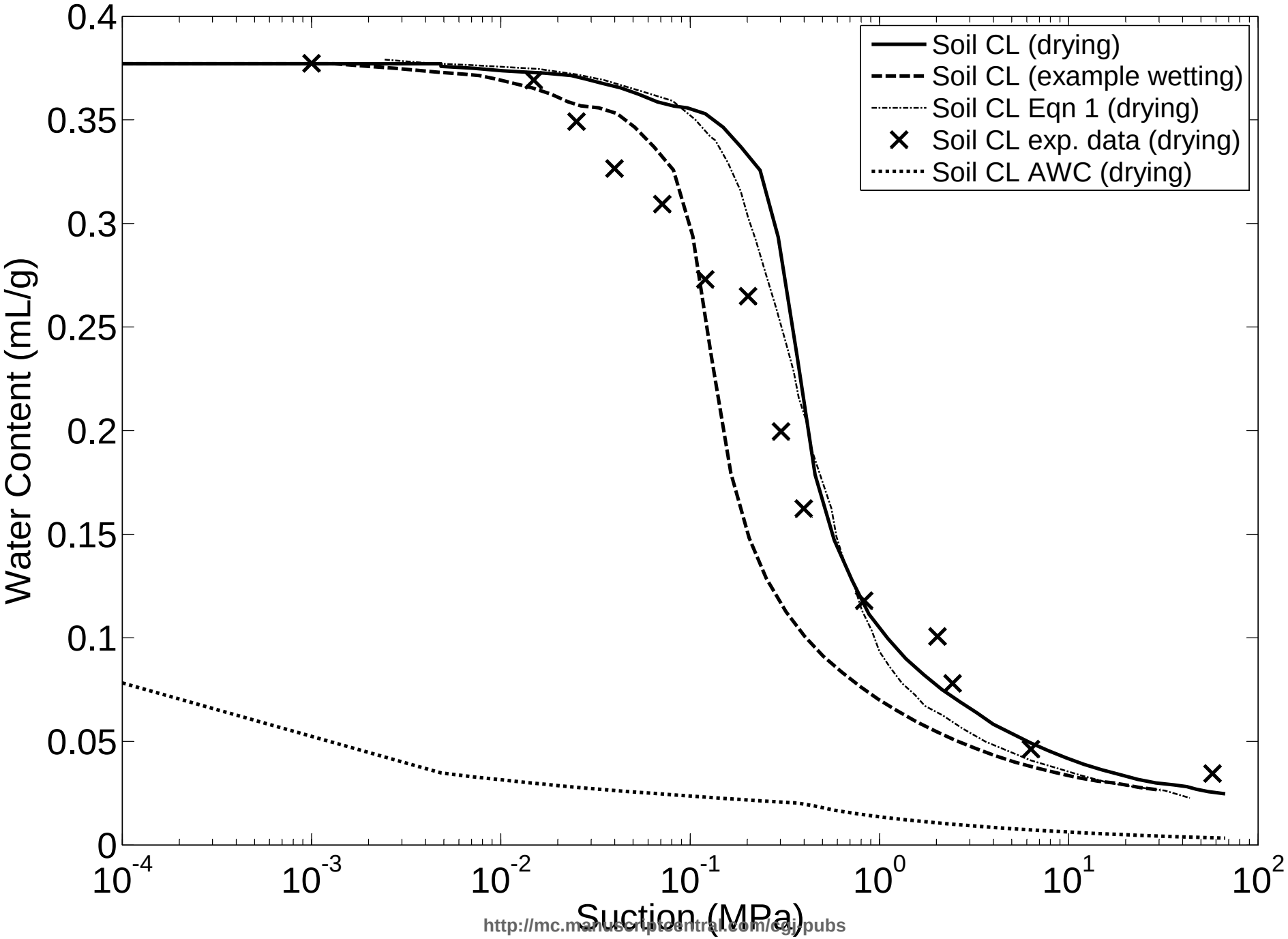
Soil CL (drying)
Soil CL (example wetting)
Soil CL Eqn 1 (drying)
Soil CL exp. data (drying)
Soil CL AWC (drying)
Water Content (mL/g)
Suction (MPa)
0.4
0.35
0.3
0.25
0.2
0.15
0.1
0.05
0
10-4
10-3
10-2
10-1
100
101
102

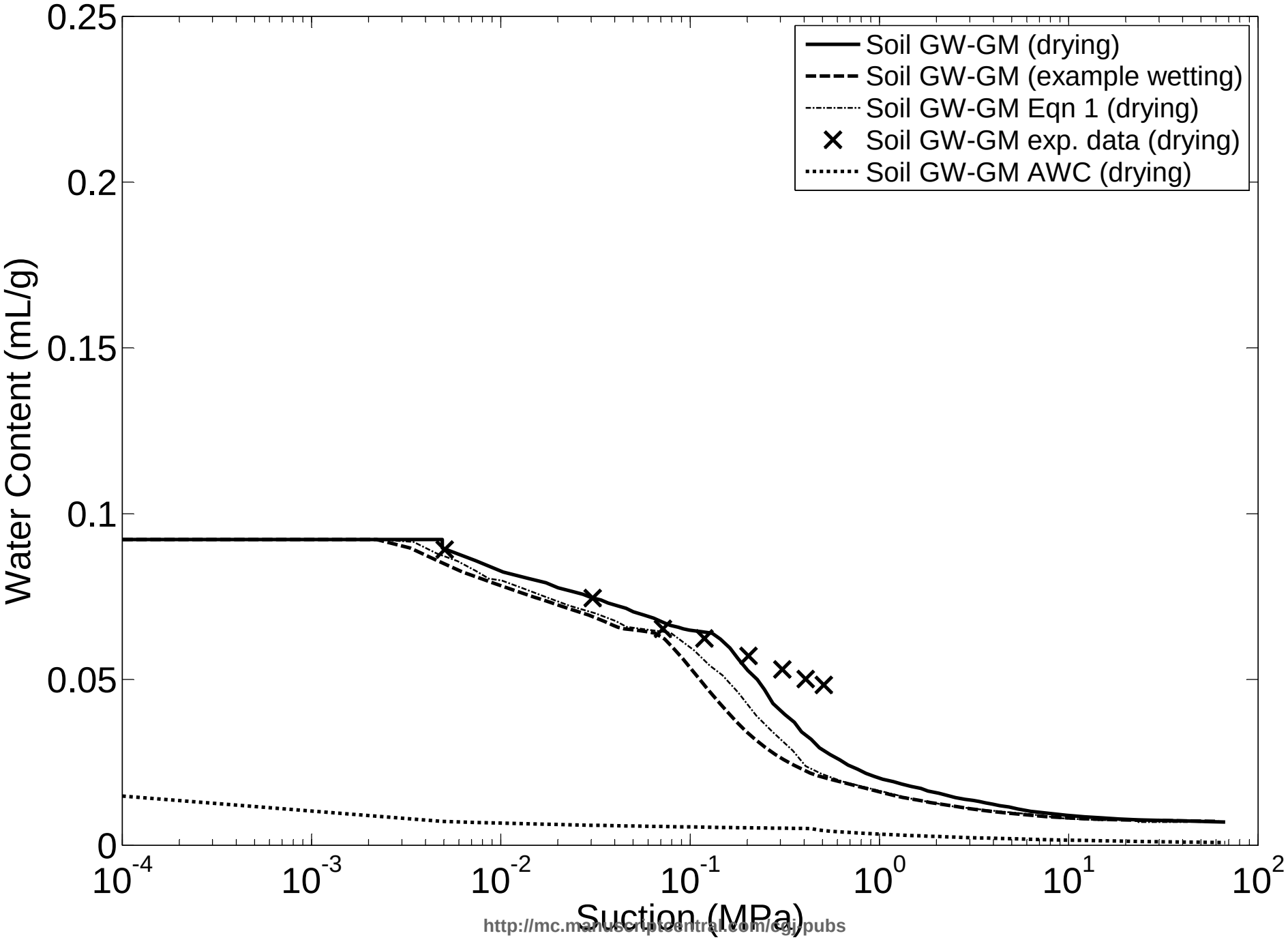

http://mc.manuscriptcentral.com/cgj-pubs

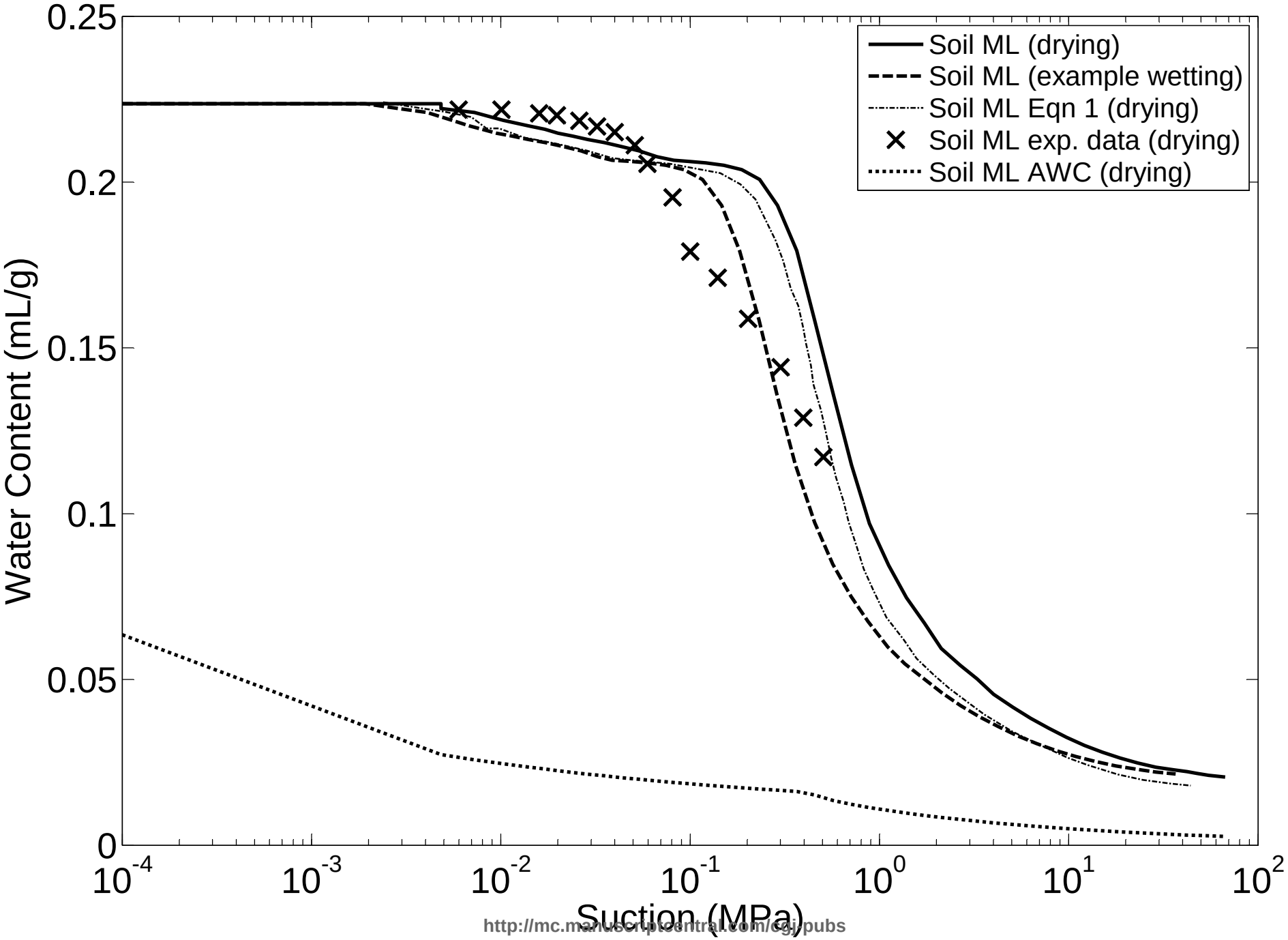

http://mc.manuscriptcentral.com/cgj-pubs

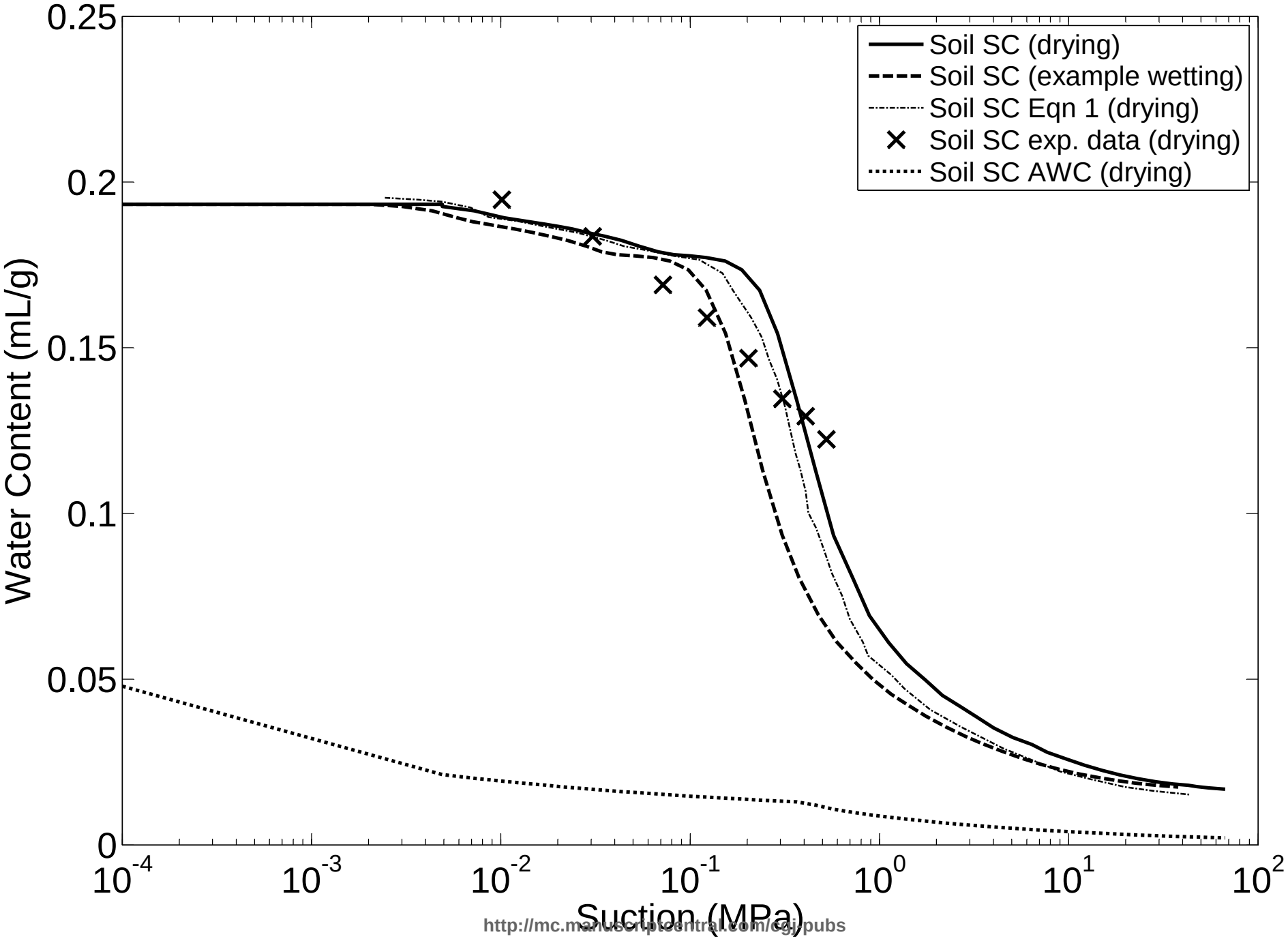

http://mc.manuscriptcentral.com/cgj-pubs

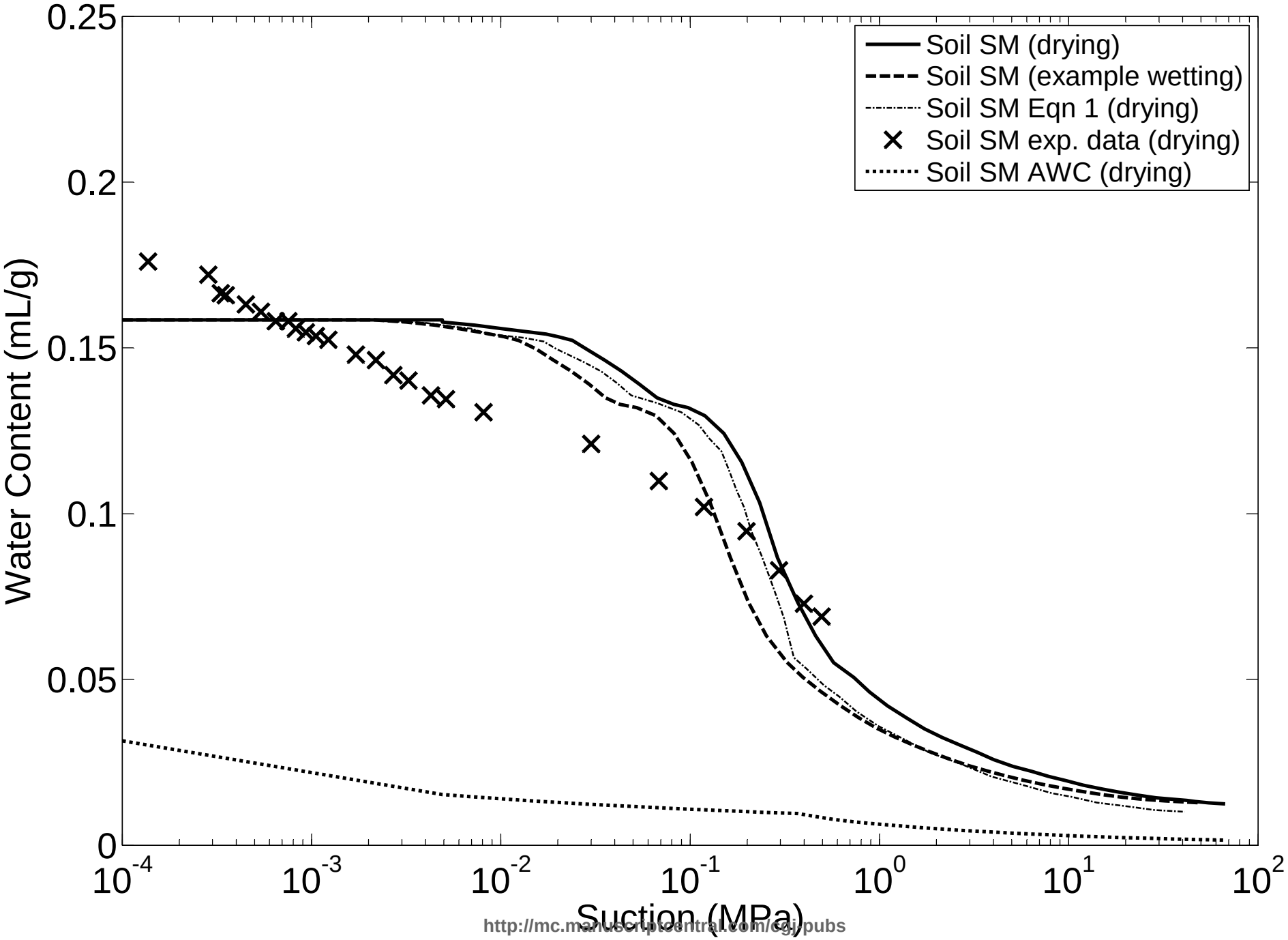

http://mc.manuscriptcentral.com/cgj-pubs

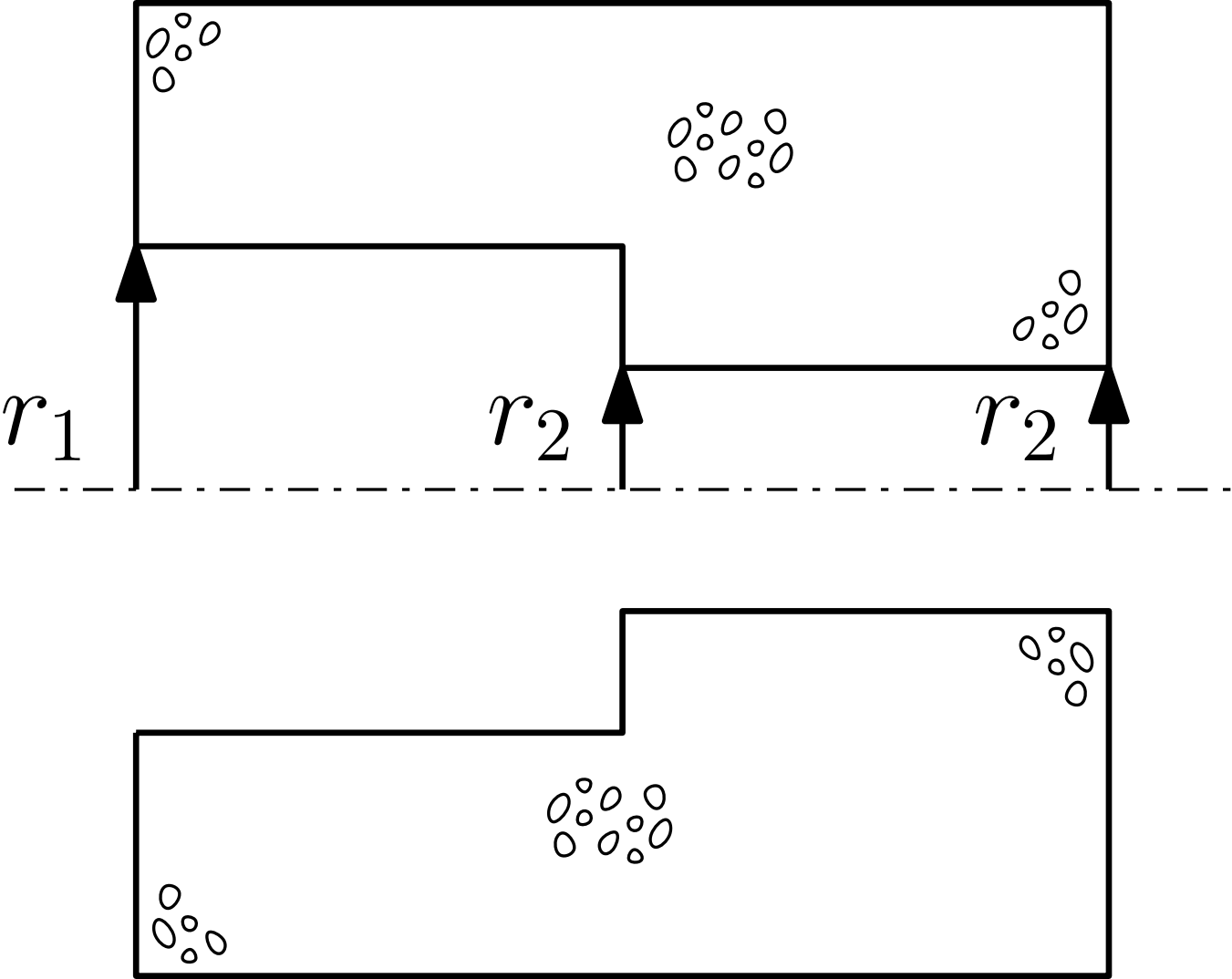
r_1
r_2
r_2

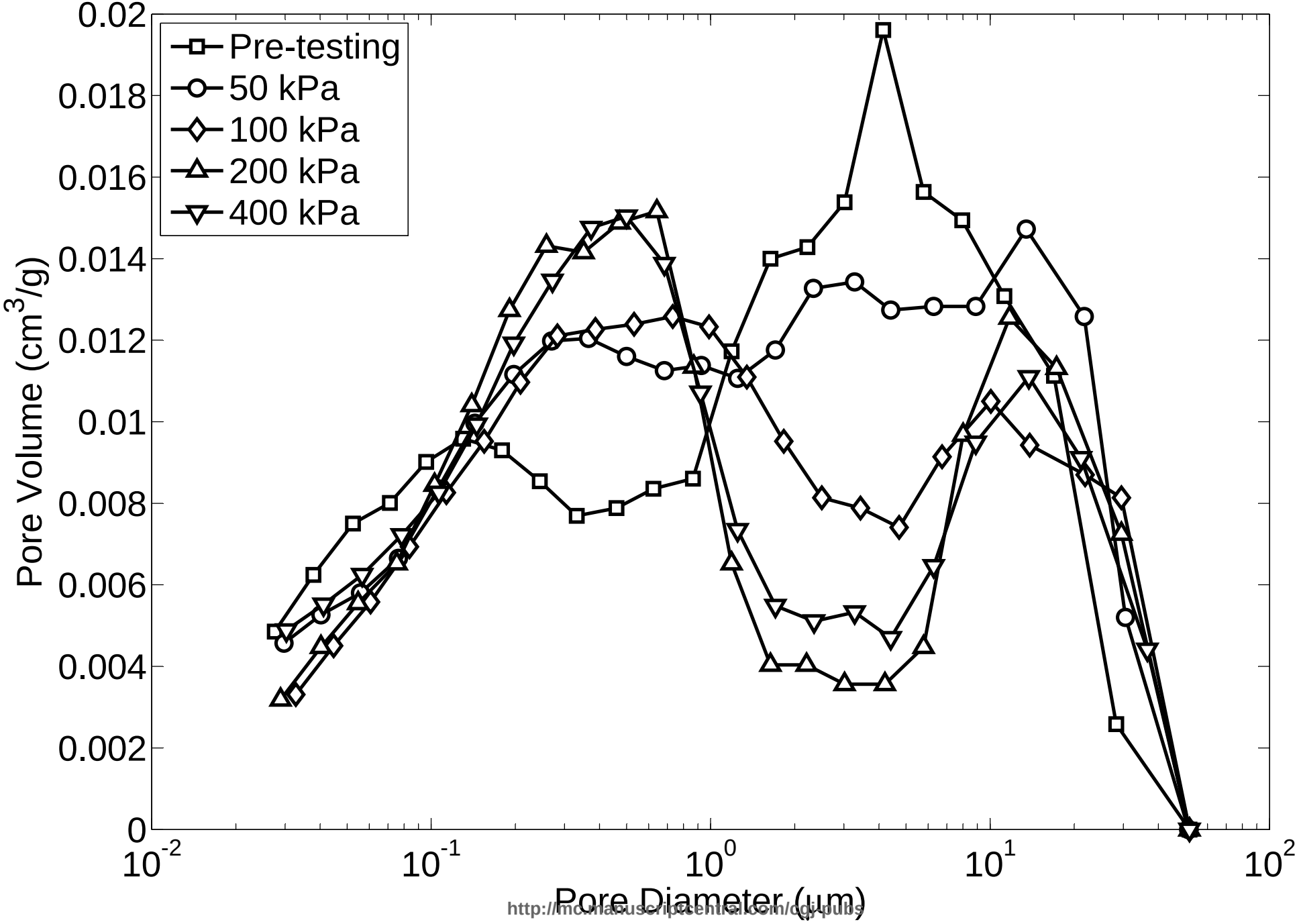

http://mc.manuscriptcentral.com/cgj-pubs

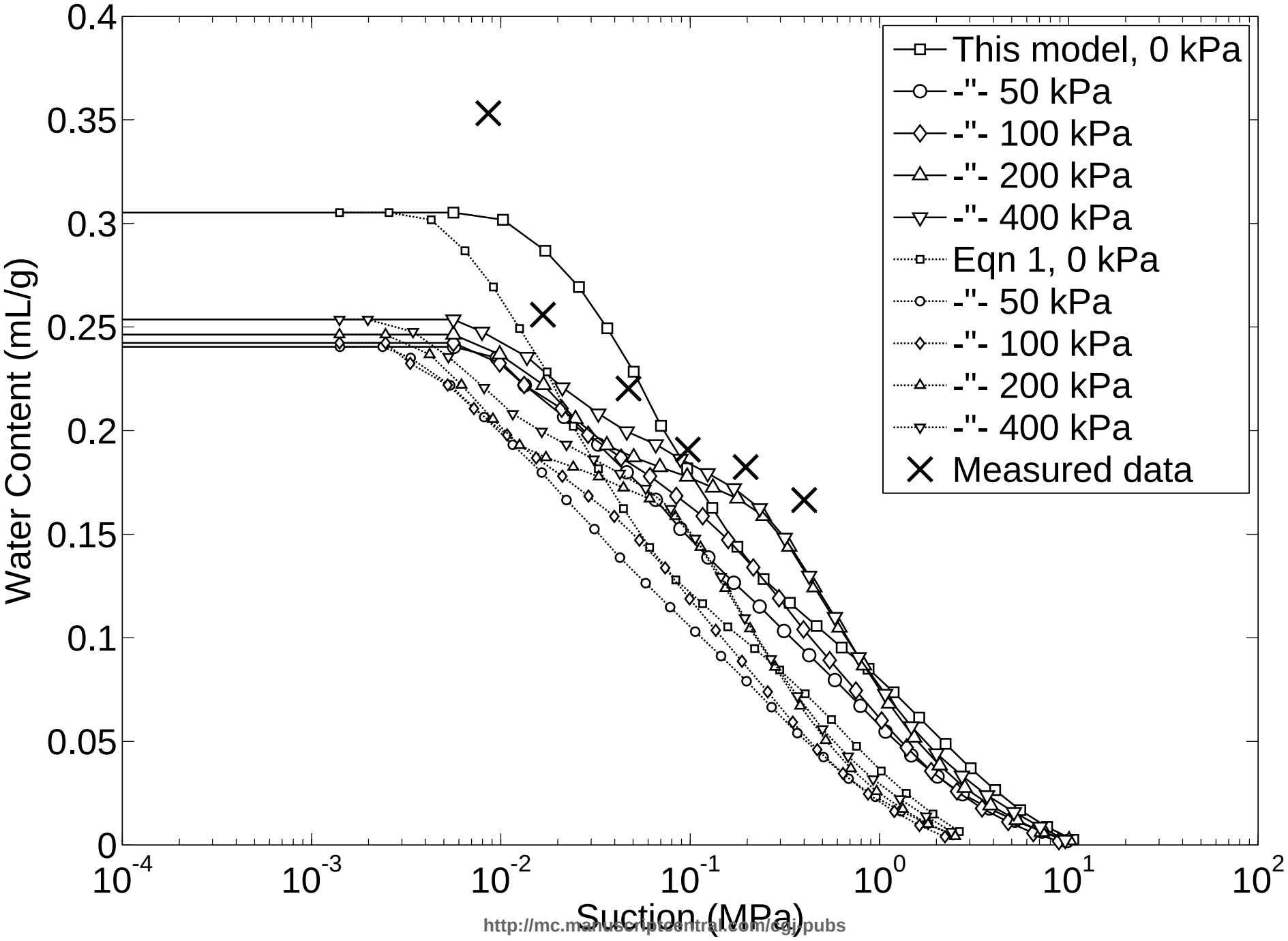

http://mc.manuscriptcentral.com/cgj-pubs